Available online at www.sciencedirect.com
ScienceDirect
Cement and Concrete Research 38 (2008) 1–18
Cement and Concrete Research

Thermodynamic modelling of the effect of temperature on the hydration and porosity of Portland cement

Barbara Lothenbach [a,*], Thomas Matschei [a,b], Göril Möschner [a], Fred P. Glasser [b]

[a] Empa, Laboratory for Concrete & Construction Chemistry, Überlandstrasse 129, CH-8600 Dübendorf, Switzerland
[b] University of Aberdeen, Department of Chemistry, Meston Walk, Old Aberdeen, AB24 3UE, Scotland, UK

Received 10 January 2007; accepted 21 August 2007

Abstract

The composition of the phase assemblage and the pore solution of Portland cements hydrated between 0 and 60 °C were modelled as a function of time and temperature. The results of thermodynamic modelling showed a good agreement with the experimental data gained at 5, 20, and 50 °C. At 5 and at 20 °C, a similar phase assemblage was calculated to be present, while at approximately 50 °C, thermodynamic calculations predicted the conversion of ettringite and monocarbonate to monosulphate.

Modelling showed that in Portland cements which have an Al_2O_3/SO_3 ratio of >1.3 (bulk weight), above 50 °C monosulphate and monocarbonate are present. In Portland cements which contain less Al (Al_2O_3/SO_3 < 1.3), above 50 °C monosulphate and small amounts of ettringite are expected to persist. A good correlation between calculated porosity and measured compressive strength was observed.

Keywords: Temperature; Thermodynamic calculations; Pore solution; Hydration products; Modeling

1. Introduction

Higher temperatures lead initially to rapid hydration of Portland cements and to high early compressive strengths [1–3]. However, the 28 and 91 day strengths of mortar and concrete samples are found to be reduced at higher temperature, although the observed degree of hydration is similar to that achieved in the temperature range 5–50 °C. At higher temperatures, the precipitating hydrates are distributed inhomogenously resulting in a coarser porosity [4], denser C–S–H, and a more equant morphology of ettringite [2]. In addition, at 50 °C or above, monosulphate is increasingly formed at the expenses of ettringite and monocarbonate [2]. Temperature also influences the composition of the pore solution. The concentrations of some ions remain little changed but sulphate concentrations increase and aluminium concentrations decrease at higher temperatures [2,5].

Thermodynamic modelling can be used to study the influence of composition and temperature on the hydrate assemblage and on the composition of the pore solution. The possibility to vary parameters systematically is a valuable tool to further our understanding of the influence of different factors such as composition or temperature on cement hydration. Thomas et al. [5] have investigated the composition of the pore solution of two different Portland cements and calculated the saturation indices of ettringite, monosulphate, gypsum and portlandite between 5 and 50 °C. Lothenbach and Winnefeld [6] and Lothenbach and Wieland [7] coupled thermodynamic modelling with a set of simple equations to describe the kinetics of cement hydration and were thus able to predict quantitatively the composition of the solid and liquid phase at 20 °C. In the title paper, the thermodynamic database has been expanded to allow calculations between 0 and 100 °C. The modelling results are compared with the experimental findings for a sulphate-resisting Portland cement (SRPC) and a Portland-limestone cement (PLC) reported by Lothenbach et al. [2]. In addition, the calculated total volumes of solids in different hydrated cements are compared to compressive strength data measured in the temperature range 5–40 °C [8] for a number of different Portland-limestone cements and an ordinary Portland cement.

* Corresponding author. Tel.: +41 44 823 47 88; fax: +41 44 823 40 35.
E-mail address: barbara.lothenbach@empa.ch (B. Lothenbach).

0008-8846/$ - see front matter © 2007 Elsevier Ltd. All rights reserved.
doi:10.1016/j.cemconres.2007.08.017

2. Materials and methods

Modelling results are compared to experimental results gained from a sulphate resistant Portland cement (SRPC): CEM I 52.5 N HTS, four different Portland-limestone cements (PLC: CEM II/A-LL 42.5 R and PLC2, PLC3, and PLC4: CEM II/A-L 32.5 R) and an ordinary Portland cement (OPC), CEM I 42.5 N. The chemical compositions of the cements were determined by X-ray fluorescence analysis (XRF) and the amount of CO_2 by TGA (Table 1). The experimental techniques as well as the compressive strength and porosity data are described in detail elsewhere [2,7,8]. Briefly, cement pastes from SRPC were prepared at *w/c* of 0.4, isothermally cured at 5, 20 and 50 °C, and the composition of the liquid and solid phase was analysed [2,7]. Mortar prisms of the cements PLC, PLC2, PLC3, PLC4 and OPC were prepared using a *w/c* of 0.58 with 3 kg quartz aggregate (0–2 mm, mixture of crushed and round quartz) per kg cement [2,8]. Mortar samples were isothermally cured for 1, 2, 7, 28, or 91 days at 5, 20, 30, or 40 °C. The specimens were demoulded after 24 h and immediately covered with plastic. The compressive strengths of the mortar samples were measured according to EN 196-1. Capillary, gel and total porosity were measured on 28-day mortar samples according to [9], where gel porosity is calculated from the difference in water content of samples dried at 50 and 110 °C. Capillary porosity is calculated from the difference in water content of saturated samples and samples dried at 50 °C: the total porosity is taken as the sum of gel and capillary porosity.

Table 1
Composition of the cements used: SRPC (CEM I 52.5 N HTS), PLC (CEM II/A-L 42.5 R), PLC2, PLC3 and PLC4 (all CEM II/A-L 32.5 R), and OPC (CEM I 42.5 N)

	SRPC	PLC	PLC2	PLC3	PLC4	OPC
Chemical analysis [g/100 g] [a]						
CaO	65.7	59.5	61.5	57.1	59.2	62.4
SiO_2	22.3	16.6	17.4	17.2	17.2	18.9
Al_2O_3	2.7	4.4	4.3	3.9	4.7	4.4
Fe_2O_3	1.9	2.4	2.3	2.0	2.5	2.5
CaO (free)	0.45	1.7	0.70	0.5	1.2	0.6
MgO	0.85	1.8	1.7	1.5	1.8	1.4
K_2O	0.22	0.83	0.87	0.78	0.81	0.95
Na_2O	0.13	0.28	0.09	0.14	0.28	0.10
CO_2	1.6	7.1	6.6	6.2	7.8	2.1
SO_3	2.2	2.5	2.7	2.9	2.5	3.0
Ignition loss		8.2	8.8	7.1	8.8	2.6
Blaine surface area [m^2/kg]	354	438	384	349	393	298
Normative phase composition [g/100 g] [b]						
Alite	61	35	44	33	25	58
Belite	18	21	17	25	30	10
Aluminate	3.9	7.6	7.4	6.9	8.2	7.6
Ferrite	5.8	7.3	7.1	6.2	7.6	7.5
CaO (free)	0.45	1.7	0.70	–	1.2	0.6
$CaCO_3$	3.7	16	15	14	18	4.8
$CaSO_4$	3.6	3.0	2.7	3.6	2.7	3.6
K_2SO_4 [c]	0.14	1.1	1.4	1.3	13	1.6
Na_2SO_4 [c]	0.09	0.23	0.10	0.14	0.28	0.10
K_2O [d]	0.14	0.25	0.09	0.08	0.09	0.10
Na_2O [d]	0.09	0.18	0.05	0.08	0.15	0.05
MgO [d]	0.85	1.8	1.7	1.5	1.8	1.4
SO_3 [d]	0.01	0.08	0.12	0.10	0.16	0.16

[a] XRF data corrected for ignition loss.
[b] Calculated from the chemical analysis.
[c] SRPC: readily soluble alkalis were calculated from the concentrations of alkalis measured in the solution after 5 min agitation at a *w/c* of 10; present as alkali sulphates. PLC and OPC: Estimated based on the alkali content and on the alkali distribution given in Taylor (1987).
[d] Present as solid solution in the major clinker phases.

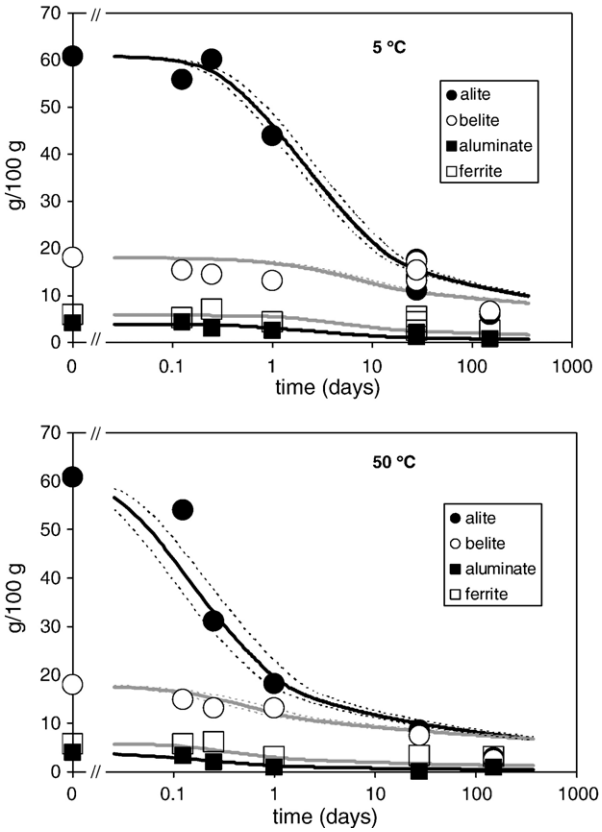

Fig. 1. Comparison of the calculated amount of clinker present in SRPC as a function of hydration time and temperature with the results of the semi-quantitative evaluation of the XRD patterns. XRD data are scaled such that the percentages in the unhydrated cement correspond to the calculated composition of the cement as given in Table 1. The results of the calculations, based on Eqs. (1)–(5) and the data given in Tables 2 and 3, displayed in bold lines. The dotted lines represent the calculations where the activation energy has been varied by ±10 kJ/mol.

3. Modelling approach

When cement is brought into contact with water, easily soluble solids such as gypsum or calcite react until equilibrium with the pore solution is reached. The clinker phases hydrate slowly releasing continuously Ca, Si, Al, Fe and hydroxide into the solution, which then precipitate as hydrates: C–S–H, ettringite, etc. The balance between dissolution rate of the clinker phases and the precipitation determines the amount of Ca, Al, Fe, Si, and hydroxide released and thus the precipitation rate of hydrates. The hydration model used in this study is described in detail by Lothenbach and Winnefeld [6] and accounts for all the reactions described above. The compositions of the solid and liquid phase are calculated as a function of time and temperature based on (i) the composition of the cement paste as given in Table 1, (ii) the

calculated degree of the dissolution of the clinkers (see below and Fig. 1) and (iii) thermodynamic calculations. For the modelling it is also assumed that alkalis originating from the dissolution of the alkali sulphates and clinker phases partition between the aqueous solution and the precipitating C–S–H phases [6,7]. To model the uptake of alkali uptake by C–S–H the same distribution ratio, R_d, of 0.42 ml/g [6,10] was used for both Na and K.

3.1. Influence of temperature on the dissolution of cement clinkers

The hydration of cements can be assumed to take place via dissolution and precipitation processes. The calculation transfers mass between clinker and hydrates by assuming dissolution and precipitation, but this does not necessarily imply a dissolution and precipitation mechanism; direct attack by water on solid clinker phases can occur and the calculations do not disclose directly the actual hydration mechanisms. Different models exist, based on quantitative X-ray measurements, to describe the dissolution of clinkers in Portland cement [11–14] as a function of time. These authors derive empirical expressions to estimate the degree of dissolution of each clinker mineral as a function of time; differences between the results of these four different approaches are generally rather small. However, the mathematical expressions used by [11,13,14] imply that essentially no dissolution of any of the clinker phases occurs during the first few hours. In contrast, the approach of Parrot and Killoh [12] has no such restrictions and describes the rate, R, of the hydration of the individual clinker phases by a set of equations, where the lowest value of R at time t is considered to be the rate-controlling step. The key equations are:

nucleation and growth $$R_t = \frac{K_1}{N_1}(1-\alpha_t)(-\ln(1-\alpha_t))^{(1-N_1)} \text{ or} \quad (1)$$

diffusion $$R_t = \frac{K_2 \times (1-\alpha_t)^{2/3}}{1-(1-\alpha_t)^{1/3}} \text{ or} \quad (2)$$

formation of hydration shell $$R_t = K_3 \times (1-\alpha_t)^{N_3} \quad (3)$$

The degree of hydration α at time t (days) is expressed as $\alpha_t = \alpha_{t-1} + \Delta t \cdot R_{t-1}$. In this paper, the empirical expressions Eqs. (1)–(3) from Parrot and Killoh [12] are used together with the values of K_1, N_1, K_2, K_3 and N_3 as compiled in Table 2. The influence of w/c according to $f(w/c) = (1 + 4.444 \cdot (w/c) - 3.333 \cdot \alpha_t)^4$; for $\alpha_t > 1.333 \cdot (w/c)$ [12] as well as the influence of the surface area on the initial hydration are included using the data given in [12].

Table 2
Parameters from Parrot and Killoh [12] used to calculate the hydration of the individual clinker phases as a function of time

Parameter[a]	Calculated clinker mineralogy			
	Alite	Belite	Aluminate	Ferrite
K_1	1.5	0.5	1.0	0.37
N_1	0.7	1.0	0.85	0.7
K_2	0.05	0.006	0.04	0.015
K_3	1.1	0.2	1.0	0.4
N_3	3.3	5.0	3.2	3.7

[a] All parameters from Parrot and Killoh [12] for OPC.

Table 3
Reported activation energies for the hydration of C_3S, C_2S, C_3A and C_4AF. Values used in the present study are printed in bold

Phase	Activation energy (kJ/mol)	System	Reference
C_3S	39	C_3S	[19]
C_3S	30	C_3S	[17]
C_3S	35–36	C_3S	[17]
C_3S	30–35	C_3S, induction and acceleration period	[17]
C_3S	37–38	C_3S, induction and acceleration period	[17]
C_3S	26	Cement	[19]
C_3S	33	Cement, presence of C_2S and C_4AF neglected	[20]
C_3S	**42**	Cement, deceleration period	[13,21]
C_2S	31	C_2S	[19]
C_2S	56	Cement	[19]
C_2S	**21**	Cement, deceleration period	[13,21]
C_3A	39–43	Cement, presence of C_2S and C_4AF neglected	[20]
C_3A	**54**	Cement	[13,21]
C_4AF	**34**	Cement	[13,21]

The effect of temperature on rate constants of chemical reactions may be expressed by the Arrhenius equation

$$R_T = Ae^{-\frac{E_a}{R \cdot T}} \quad (4)$$

where parameter A is independent of, or varies little, with temperature and E_a is the apparent activation energy [J/mol]. The rate at temperature of interest is then calculated by

$$R_{t,T} = R_{t,T_0} e^{-\frac{E_a}{R}\left(\frac{1}{T}-\frac{1}{T_0}\right)} \quad (5)$$

where T corresponds to the temperature of interest in K, T_0 to 293 K (20 °C) and $R_{t,T0}$ to the rate at time t calculated at 20 °C (cf. Eqs. (1)–(3)).

Reported activation energies for cement hydration generally range from 35 to 50 kJ/mol [15–18]. Reported activation energies for the different clinker phases are spread over similar broad range of values; for alites activation energies from 26 to 42 kJ/mol have been reported [13,17,19–21] (cf. Table 3). The specific surface area of the investigated sample influences the measured activation energies [22]; in addition, values measured in pure systems may differ from those determined in multiphase cementitious systems [19]. The dataset derived in [13,21] is used in the present paper for modelling the cement hydration as this dataset is based on measurements made on cements and includes data for all four principal clinker phases (Table 3)). The exact values of activation energies used in the hydration modelling are of minor importance as the calculated degree of hydration is not strongly dependent on the numerical value of the activation energy. Even a variation of the activation energy by ±10 kJ/mol results in relatively small changes in the calculated degree of hydration during the first day, as indicated by the dotted lines in Fig. 1 for alite and belite. At longer hydration times, these differences decrease.

Table 4
Standard thermodynamic properties at 25 °C: Thermodynamic data for cements "cemdata2007"

	log K^{a}_{s0}	$\Delta_f G°$ [kJ/mol]	$\Delta_f H°$ [kJ/mol]	$S°$ [J/K/mol]	a_0 [J/K/mol]	a_1	a_2	a_3	$V°$ [cm^3/mol]
(Al-)ettringite	−44.9[b]	−15205.94[b]	−17535[b]	1900[b]	1939[c]	0.789[c]			707[d]
Tricarboaluminate	−46.5[f]	−14565.64[f]	−16792[b]	1858[b]	2042[b]	0.559[b]	−7.78e6[b]		650[d]
Fe-ettringite	−44.0[g]	−14282.36[g]	−16600[g]	1937[g]	1922[g]	0.855[g]	2.02e6[g]		717[h]
C_3AH_6	−20.84[f]	−5010.09[f]	−5540[f]	419[f]	292[c]	0.561[c]			150[d]
$C_3AS_{0.8}H_{4.4}$*	−29.87[f]	−5368.01[f]	−5855[f]	369[f]	109[f]	0.631[f]	−1.95e6[f]	2560[f]	143[f]
C_3FH_6**	−25.16[b]	−4116.29[b]	−4640[b]	439[b]	275[b]	0.627[b]	2.02e6[b]		155[d]
C_4AH_{13}	−25.40[b]	−7326.56[b]	−8302[b]	700[b]	711[b]	1.047[b]		−1600[b]	274[d]
C_2AH_8	−13.56[b,i]	−4812.76[b,i]	−5433[b]	440[b]	392[b]	0.714[b]		−800[b]	184[d]
$C_4A\bar{S}H_{12}$	−29.26[f]	−7778.50[f]	−8750[f]	821[f]	594[c]	1.168[c]			309[d]
$C_4A\bar{C}H_{11}$	−31.47[f,i]	−7337.46[f,i]	−8250[f]	657[f]	618[b]	0.982[b]	−2.59e6[b]		262[d]
$C_4A\bar{C}_{0.5}H_{12}$	−29.13[f]	−7335.97[f]	−8270[f]	713[f]	664[b]	1.014[b]	−1.30e6[b]	−800[b]	285[d]
C_2ASH_8	−19.70[f]	−5705.15[f]	−6360[f]	546[f]	438[b]	0.749[b]	−1.13e6[b]	−800[b]	216[d]
C_4FH_{13}**	−29.4[b]	−6430.94[b]	−7395[b]	737[b]	694[b]	1.113[b]	2.02e6[b]	−1600[b]	286[d]
C_2FH_8**	−17.6[b]	−3917.38[b]	−4526[b]	476[b]	375[b]	0.780[b]	2.02e6[b]	−800[b]	194[d]
$C_4F\bar{S}H_{12}$	−33.2[g]	−6882.55[g]	−7843[g]	858[g]	577[g]	1.234[g]	2.02e6[g]		322[j]
$C_4F\bar{C}H_{12}$**	−35.5[g]	−6679.20[g]	−7637[g]	737[g]	612[g]	1.157[g]	−5.73e5[g]		290[k]
$C_4F\bar{C}_{0.5}H_{12}$**	−33.1[b]	−6440.19[b]	−7363[b]	749[b]	648[b]	1.080[b]	7.24e5[b]	−800[b]	296[d]
$C_2F\bar{S}H_8$**	−23.7[b]	−4809.53[b]	−5453[b]	583[b]	422[b]	0.815[b]	8.91e5[b]	−800[b]	227[d]
M_4AH_{10}**	−56.02[i]	−6394.56[i]	−7196[b]	549[b]	−364[b]	4.21[b]	3.75e6[b]	629[b,l]	220[m]
M_4AcH_9**	−51.14[i]	−6580.15[b]	−7374[b]	551[b]	−382[b]	4.24[b]	4.32e6[b]	629[b,l]	220[n]
M_4FH_{10}**	−60.0[b]	−5498.84[b]	−6289[b]	586[b]	−381[b]	4.27[b]	5.78e6[b]	629[b,l]	232[o]
$C_{1.67}SH_{2.1}$(jen.)	−13.17[b,i]	−2480.81[b]	−2723[b]	140[b]	210[b]	0.120[b]	−3.07e6[b]		78[b,d]
$C_{0.83}SH_{1.3}$(tob.)	−8.0 [b]	−1744.36[b]	−1916[b]	80[b]	85[b]	0.160[b]			59[b]
portlandite	−5.20[p]	−897.01[p]	−985[p]	83[p]	187[p]	−0.022[p]		−1600[p]	33[p]
SiO_2,am	1.476[p]	−848.90[p]	−903[q]	41[q]	47[q]	0.034[q]	−1.13e6[q]		29[p]
H_2O	−14.00[p]	−237.18[p]	−286[p]	70[p]	75[p]				18[p]
Gypsum	−4.58[p]	−1797.76[p]	−2023[p]	194[p]	91[p]	0.318[p]			75[p]
Anhydrite	−4.36[p]	−1322.12[p]	−1435[p]	107[p]	70[p]	0.099[p]			46[p]
Calcite	−8.48[p]	−1129.18[p]	−1207[p]	93[p]	105[p]	0.022[p]	−2.59e6[p]		37[p]
Brucite	−11.16[p]	−832.23[p]	−923[p]	63[p]	101[p]	0.017[p]	−2.56e6[p]		25[p]
$Al(OH)_3$(am)	0.24[i]	−1143.21[i]	−1281[b]	70[p]	36[p]	0.191[p]			32[p]
Al_2O_3	1.64[r]	−1568.26[r]	−1662[r]	51[r]	115[r]	0.012[r]	−3.51e6[r]		26[r]
$Fe(OH)_3$(mic)	−4.60[i]	−711.61[i]	−844b	88[b]	28[b]	0.052[b]			34[b]
Fe_2O_3	−14.08[p]	−739.53[p]	−821[p]	88[p]	98[p]	0.078[p]	−1.49e6[p]		30[p]
C_3S		−2784.33[s]	−2931[s]	169[s]	209[s]	0.036[s]	−4.25e6[s]		73[d]
C_2S		−2193.21[s]	−2308[s]	128[s]	152[s]	0.037[s]	−3.03e6[s]		52[d]
C_3A		−3382.35[s]	−3561[s]	205[s]	261[s]	0.019[s]	−5.06e6[s]		89[d]
C_4AF		−4786.50[s]	−5080[s]	326[s]	374[s]	0.073[s]			130[d]

a_0, a_1, a_2, a_3 are the empirical coefficients of the heat capacity equation: $C_p^\circ = a_0 + a_1T + a_2T^{-2} + a_3T^{-0.5}$; no value = 0.
[a]All solubility products refer to the solubility with respect to the species $Al(OH)_4^-$, $Fe(OH)_4^-$, $SiO(OH)_3^-$, OH^-, H_2O, Ca^{2+}, Mg^{2+}, CO_3^{2-}, or SO_4; [b] This paper, see Appendix; [c] Data measured by Ederova [30], [d] Molar volume $V°$ calculated from unit cell or densities given in Taylor [31]; [f] Matschei et al. [27,28]; [g] Möschner et al. [29]; [h] calculated from crystallographic unit cell given by McMurdie et al. [32]; [i] Lothenbach and Winnefeld [6]; [j] calculated from [33]; [k] alculated from [34]; [l] $C_p° = a_0 + a_1T + a_2T^{-2} + a_3T^{-0.5} - 0.00424*T^2 + 2.11E-6*T^3$; [m]calculated from Mascolo et al. [35]; [n] Bellotto et al. [36]; [o] estimated from Sato et al. [37]; [p] from PSI-GEMS dataset [24,25], $S°$ and C_p° for $Al(OH)_3$(am) are taken from $Al(OH)_3$(gibbsite); [q] $S°$ and C_p° for SiO_2(am) are taken from SiO_2(quartz), c.f. Kulik and Kersten [38]; [r]Helgeson et al. [39]; [s]Babushkin et al. [40]. * not considered in the present calculations as it precipitates very slowly. ** tentative values.

The set of equations used (Eqs. (1)–(5)) describes well the progress of dissolution at 5, 20, and 50 °C of the cements investigated, as can be seen by comparing the calculated progress of dissolution with the results of the semi-quantitative XRD (Fig. 1). In accordance with the measured data, the calculated progress of hydration at 50 °C is initially fast but slows, while at 5 °C the calculated progress of hydration starts at a much slower rate but progresses more steadily so that the calculated hydration degrees at 5 and at 50 °C are similar by 150 days.

3.2. Thermodynamic model and data

In this paper, thermodynamic modelling is carried out using the Gibbs free energy minimisation program GEMS-PSI [23]. GEMS-PSI is a broad-purpose geochemical modelling code which computes equilibrium phase assemblage and speciation in a complex chemical system from its total bulk elemental composition. Chemical interactions involving solids, solid solutions, and aqueous electrolyte are considered simultaneously. The speciation of the dissolved species as well as the kind and amount of solids precipitated are calculated. In contrast to the solid solution calculation features implemented in the well-known speciation code PHREEQC, the code GEMS-PSI can predict the compositions of solid solutions and the coexisting liquid phase based on the bulk chemical composition of the system. Thermodynamic data for aqueous species, as well as for many solids, were taken from the GEMS-PSI thermodynamic database [24,25], see Table 4. The constants given in the

original PSI thermodynamic database [25] have been converted into standard molar Gibbs energies and merged with *slop98.dat* database [26]. This database, included in the current software package, *GEMS version 2.1*, is documented in [24]. For aqueous species, this dataset includes the HKF (Helgeson–Kirkham–Flowers) equation of state which is used to calculate temperature and pressure corrections up to 1000 °C and 5 kbar. Solubility products for cement minerals at 25 °C were taken from the compilation of Lothenbach and Winnefeld [6] and completed with the data recently determined by Matschei et al. [27,28] and Möschner et al. [29]. Thermodynamic data for extrapolation to temperatures other than 25 °C were estimated as described in the Appendix, resulting in the set of thermodynamic data for cements as given in Table 4: "cemdata2007".

The thermodynamic data for solids between 0 and 100 °C and at $P=1$ bar were calculated using the temperature dependence of the apparent Gibbs free energy of formation from element $\Delta_a G^o$ according to:

$$\begin{aligned} \Delta_a G^o_T &= \Delta_f G^o_{T_0} - S^o_{T_0}(T-T_0) - \int_{T_0}^{T}\int_{T_0}^{T}\frac{C^o_p}{T}\mathrm{d}T\mathrm{d}T \\ &= \Delta_f G^o_{T_0} - S^o_{T_0}(T-T_0) - a_0\left(T\ln\frac{T}{T_0} - T + T_0\right) \\ &\quad -0.5a_1(T-T_0)^2 - a_2\frac{(T-T_0)^2}{2T\cdot T_0^2} - a_3\frac{2(\sqrt{T}-\sqrt{T_0})^2}{\sqrt{T_0}} \end{aligned} \quad (6)$$

[41] where a_0, a_1, a_2, and a_3 are the empirical coefficients of the heat capacity equation $C_p^o = a_0 + a_1 T + a_2 T^{-2} + a_3 T^{-0.5}$ and T_0 is the reference temperature (298.15 K). The apparent Gibbs free energy of formation $\Delta_a G^o_{T0}$ refers to the free energies of the elements at 298 K. The above calculation is built into the GEMS-PSI code. A more detailed description of the derivation of the dependence of temperature of the Gibbs free energy is given in the online documentation of GEMS [23], by Kulik [42] or by Anderson and Cerar [41].

4. Modelling results and discussion

4.1. Comparison with experimental results

4.1.1. Solid phases

The model calculations predict similar degrees of hydration after 100 and more days independent of temperature (see Fig. 1), although Eq. (5) does not consider the impact upon kinetics of denser hydration rims, as observed at higher temperatures [2,43,44]. This indicates that the observed slowing of hydration after the first days at higher temperature is not only caused by the hindrance of diffusion by denser hydration rims. The experimentally observed slowing of hydration at higher temperatures may also result from the particle size distribution of the clinkers (after some time, mostly larger particles are present which hydrate very slowly) and by the limited amount of water available after longer hydration times. However, it should be noted, that a dissolution model based on the Arrhenius equation, as used here, will not be able to reproduce the crossover of the degree of hydration observed, for example, by Escalante-Garcia and Sharp [1]. The use of the Arrhenius equation implies that higher temperatures always lead to a higher degree of the dissolution even though the actual values need not differ by much.

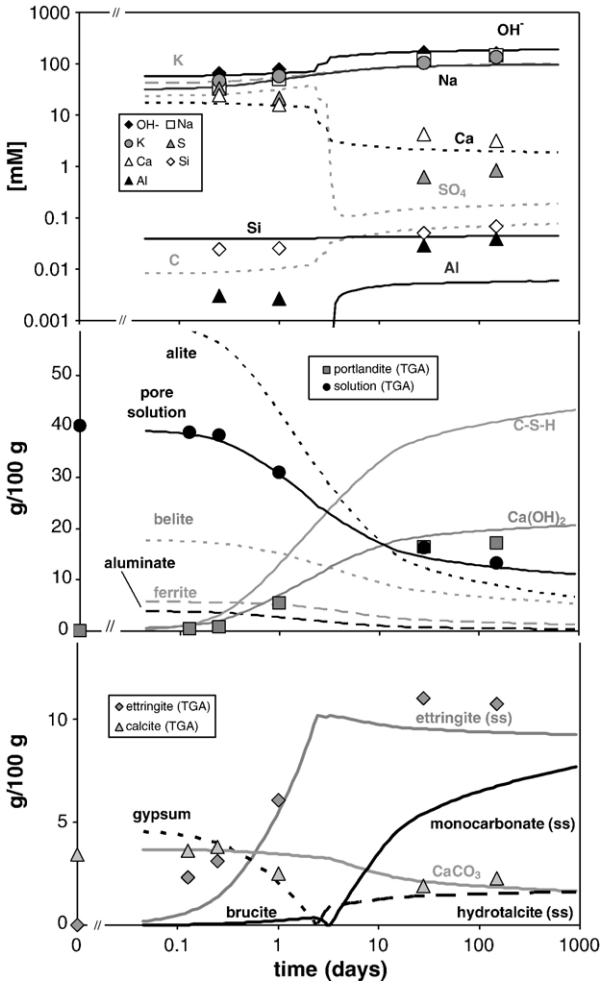

Fig. 2. Modelled evolution of the liquid and solid phases during the hydration of SRPC at $w/c=0.4$ at 5 °C compared to the experimentally determined concentrations in the pore solution and the measured amount of pore solution, portlandite, ettringite and calcite [2]. In order to ease the comparison with XRD and TGA data, the values refer to 100 g of solid; i.e. the mass of the solid phase increases with time as more and more hydration product precipitates and the amount of pore solution is reduced (ss=solid solution).

The calculated hydrate assemblage and species concentrations in the pore solution of SRPC are shown as lines in Figs. 2 and 3; experimental data [2] are given as data points. Comparison indicates a good agreement between the experimental data reported by Lothenbach et al. [2] and the calculated data. Both the calculated and the measured data show similar trends indicating that the samples are at or close to equilibrium and that the important parameters have been included in the calculations. Similarly, the comparison of the calculated amounts of portlandite, calcite, and pore solution with the amount measured by TGA show good agreement (Figs. 2 and 3).

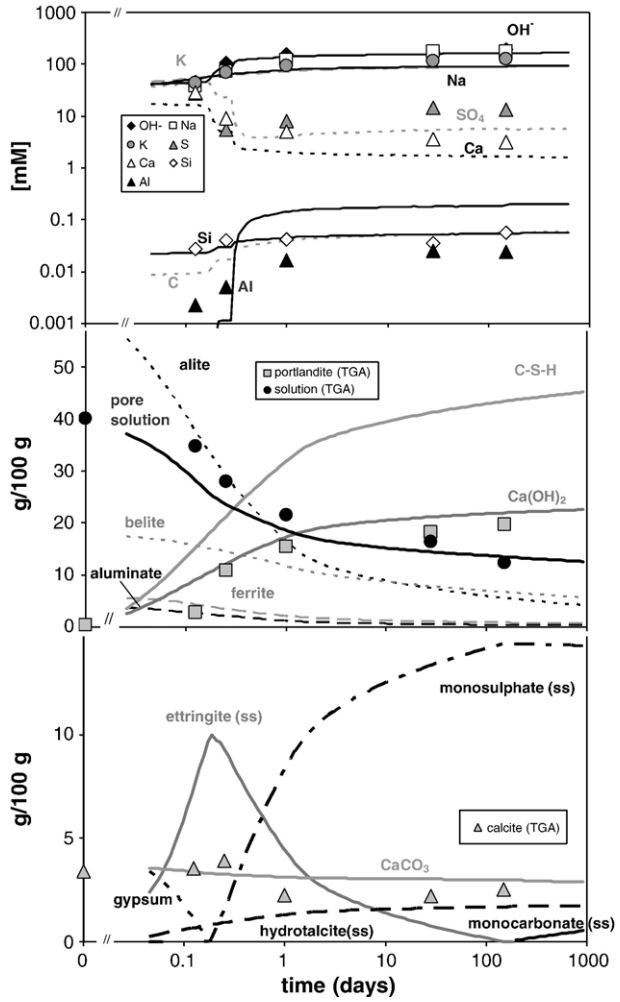

Fig. 3. Modelled evolution of the liquid and solid phases during the hydration of SRPC at $w/c = 0.4$ at 50 °C compared to the experimentally determined concentrations in the pore solution and the measured amount of pore solution, portlandite and calcite [2]. In order to ease the comparison with XRD and TGA data, the values refer to 100 g of solid; i.e. the mass of the solid phase increases with time as more and more hydration product precipitates and the amount of pore solution is reduced (ss = solid solution).

At 5 °C, the thermodynamic equilibria calculations predict the presence of C–S–H, portlandite, ettringite[1], monocarbonate and hydrotalcite; the same phase assemblage as calculated at 20 °C (see [8]). The Fe present is predicted to precipitate mainly as solid solution with Al in monocarbonate and hydrotalcite, while ettringite is predicted to contain mainly Al, as Fe-ettringite is not very stable compared to the other hydrates (see Table 4 and Appendix). Calculated concentrations in the pore solution are constant during the first two days until gypsum and anhydrite are consumed; thereafter sulphate and calcium concentrations decrease while hydroxide and aluminium concentrations increase strongly (Fig. 2).

At 50 °C, thermodynamic calculations predict the formation of monosulphate at the expense of ettringite and monocarbonate (Fig. 3), which agrees well with experimental observations [2], where a significant decrease of the amount of ettringite, the absence of monocarbonate and the presence of monosulphate has been observed at 50 °C. Christensen et al. [45] observed the start of the transformation of ettringite to monosulphate at 48 °C in a white Portland cement sample, which agrees well with our observations and calculations. The conversion of ettringite to monosulphate depends, as discussed by Glasser et al. [46], not only on temperature but also on the concentrations of Al, Ca, sulphate and hydroxide in solution. Thus ettringite in equilibrium with water or diluted NaOH may be stable up to 75 °C or higher [47,48], but in cement systems where high concentrations of alkalis are present, the amount of sulphate is rather limited and the Al/sulphate ratio is high, ettringite may already convert to monosulphate around 50 °C.

The thermodynamic calculations predict the conversion of ettringite to monosulphate at ~ 48 °C for the cement systems investigated. The thermodynamic calculations assume an equilibrium throughout the sample and a homogeneous distribution of hydrates and therefore predict complete transformation of a hydrate into another within a narrow temperature range of approximately 1 °C. In real samples, however, where the hydrates are distributed rather inhomogeneously, slightly different local equilibria can exist such that different hydrates may occur in the same sample, spreading the transformations over a broader range of temperature than predicted by the calculations. In addition, in real cement systems, AFm-phases may have a variable composition; the existence of solid solutions would remove the restriction of invariance and thus enable the transformation to occur over a range of temperatures. The exact temperature at which the transformation of monosulphate to ettringite is predicted depends very strongly on the thermodynamic data used and small changes in these data shift the predicted temperature. If a possible inaccuracy of the solubility products of ±0.1 log units is taken into account, the transformation of ettringite and monocarbonate to monosulphate is calculated to be in the temperature range 42–54 °C. But even though it is difficult to predict the exact temperature of this transformation, experimental evidence indicates that such a transformation occurs around 50 °C.

4.1.2. Pore solutions

Both, calculated and measured concentrations in the pore solution show consistent trends and agree well (Figs. 2 and 3). At 50 °C a faster initial hydration process is observed than at 5 °C, resulting in a faster change in the composition of the pore solution. After 28 and 150 days hydration, however, the concentrations in the pore solutions are similar at all temperatures with the notable exception of sulphate and aluminium, where the calculated concentrations increase markedly at higher temperatures owing to increased solubility of ettringite ([47]; see also Appendix). The comparable concentrations of alkalis

[1] For the modelling the formation of ideal solid solution between Al- and Fe-containing analogues has been assumed, see Appendix. Thus, the expressions ettringite ($Ca_6(Al,Fe)_2(SO_4)_3(OH)_{12}\cdot 26H_2O$), monocarbonate ($3CaO\cdot(Al,Fe)_2O_3\cdot CaCO_3\cdot 11–12H_2O$), monosulphate ($3CaO\cdot(Al,Fe)_2O_3\cdot CaSO_4\cdot 12H_2O$), hemicarbonate ($3.5CaO\cdot(Al,Fe)_2O_3\cdot 0.5CaCO_3\cdot 12H_2O$) or hydrotalcite ($Mg_4(Al,Fe)_2(OH)_{14}\cdot 3H_2O$) in this paper all refer to the solid solution between the Al- and Fe-containing analogues.

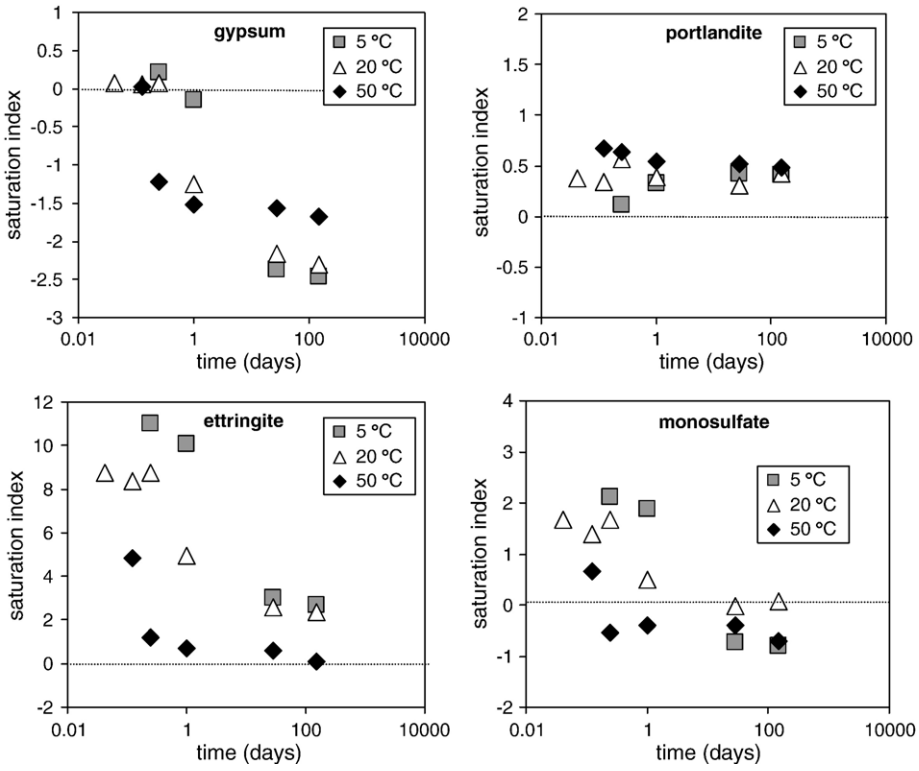

Fig. 4. Gypsum, portlandite, (Al-)ettringite and monosulphoaluminate saturation index calculated from the data of Lothenbach et al. [2] as a function of hydration time. A saturation index of 0 indicates equilibrium between liquid and solid.

present after 150 days at all temperatures agree with the observations that, after 150 days, a similar degree of hydration is reached.

The pore solutions are slightly oversaturated with respect to portlandite at all temperatures (Fig. 4) and are initially saturated or slightly oversaturated with respect to gypsum. At and above ~ 50 °C, anhydrite is thermodynamically more stable in the pore solution than gypsum. The difference, however, is small and conversion between gypsum and anhydrite is slow and, moreover, as hydration progresses, calcium sulfate is consumed. Thus, after the first few hours (50 °C) or the first days (5 °C), gypsum and anhydrite are depleted and the solutions become undersaturated with respect to calcium sulfate. The saturation index with respect to a solid is given by $\log(IAP/K_{S0})$, where IAP refers to the ion activity product (calculated from activities derived from the concentrations determined in the solution) and K_{S0} signifies the solubility product of the respective solid. A positive saturation index implies oversaturation, a negative value undersaturation with regard to the respective solid. Calculated saturation indices with respect to (Al-)ettringite are initially very high (Fig. 4), but decrease after several hours when all gypsum is consumed. The pore solutions at 5 and 25 °C are initially also oversaturated with respect to monosulphoaluminate although the numerical value of the oversaturation decreases with time. The final oversaturation is much higher with respect to iron-free ettringite indicating that ettringite is the stable phase at 5 and 25 °C. The oversaturation of ettringite is observed to decrease with increasing hydration temperature, which agrees with the findings of Thomas et al. [5]. High oversaturation may arise from a kinetic restraint for the formation of a phase, but at higher temperatures such restraints are easily overcome. Thus, the declining level of oversaturation with increasing temperatures is consistent with a kinetic restraint on ettringite formation. Although it has been observed in many investigations that the pore solutions of Portland cement are significantly oversaturated with respect to ettringite [5–7,49], the source of the kinetic barrier is unknown. In a "pure" system, i.e. just in the presence of aluminium, calcium, alkalis, sulphate, and hydroxide, saturation with respect to ettringite is reached within a few days [47]. The fact that oversaturation with respect to ettringite is observed in cement systems but not in pure systems indicates that either the presence of another ion in the pore solution or the low Al/Ca and Al/sulphate ratio hinders the precipitation of ettringite.

4.2. Hydrates formed at different temperature: SRPC

Thermodynamic modelling can also be used to calculate the hydrate assemblage after a given hydration time as a function of temperature. The hydrate assemblage of SRPC after approximately 150 days was calculated between 0 and 60 °C (Fig. 5). To facilitate comparison between different temperatures, an equal degree of hydration was assumed at all temperature. After 150 days the calculated overall degree of hydration corresponded to ~ 80%.

Portlandite, C–S–H, hydrotalcite, and calcite are calculated to be stable throughout and to be present in comparable amounts at all temperatures, which is consistent with the experimental observations. Above 48 °C, monosulphate is

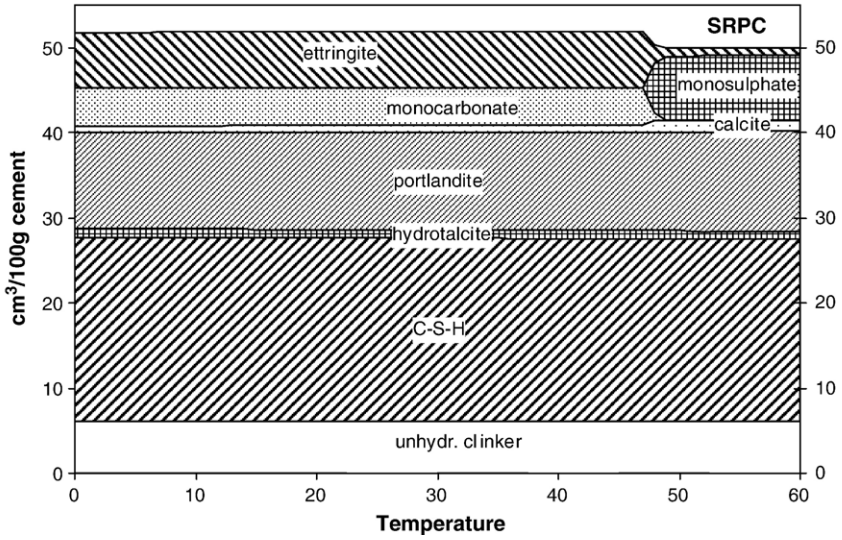

Fig. 5. Calculated volume of hydrates in SRPC as a function of temperature assuming an equal dissolution of the clinker phases.

predicted to be more stable than monocarbonate and ettringite: $Ca_6Al_2(SO_4)_3(OH)_{12}\cdot 26H_2O + 2\ [3CaO\cdot Al_2O_3\cdot CaCO_3\cdot 11H_2O] \Leftrightarrow 3\ [3CaO\cdot Al_2O_3\cdot CaSO_4\cdot 12H_2O] + 2CaCO_3 + 18H_2O$.

The relatively low molar Al_2O_3/SO_3 ratio of SRPC, 0.95 mol/mol, leads to the presence of monosulphate with the surplus of sulphate appearing as ettringite. These changes in composition of the hydrate assemblage influence the total volume of the hydrated cement (Fig. 5). The disappearance of ettringite, with its relatively low density and high molecular volume, leads to a lower total volume of the hydrated cement at higher temperature. These changes lead to increased porosity and decreased compressive strength (see also below).

4.3. Hydrates formed at different temperature: PLC

The composition of the hydrate assemblage of the Portland-limestone cement PLC hydrated for 150 days (degree of hydration corresponded to ~ 85%) calculated as a function of temperature is shown in Fig. 6. Again for all temperatures a constant degree of hydration was used. Analogous to the SRPC, at 48 °C and above, ettringite and monocarbonate are calculated to be unstable relative to monosulphate. In contrast to SRPC, monocarbonate rather than ettringite is predicted to remain above 48 °C because PLC has a high molar Al_2O_3/SO_3 ratio, of 1.39. In the presence of monosulphate, which has a theoretical molar Al_2O_3/SO_3 ratio of 1 mol/mol (or 1.3 g/g, expressed in weight), a surplus of Al is present in the system. One part of the Al is calculated to precipitate as hydrotalcite. But on the account of the low Mg contents, the remaining Al precipitates as monocarboaluminate.

Modelling enables the differences between the two cements to be quantified. Relative to SRPC, and at 20 °C, PLC is calculated to have less unhydrated clinker, as it has a higher *w/c* ratio, more calcite, more monocarbonate, more hydrotalcite but less portlandite and C–S–H; amounts of ettringite are similar. This agrees with the experimental findings presented by Lothenbach et al. [2] and gives further confirmation that the thermodynamic

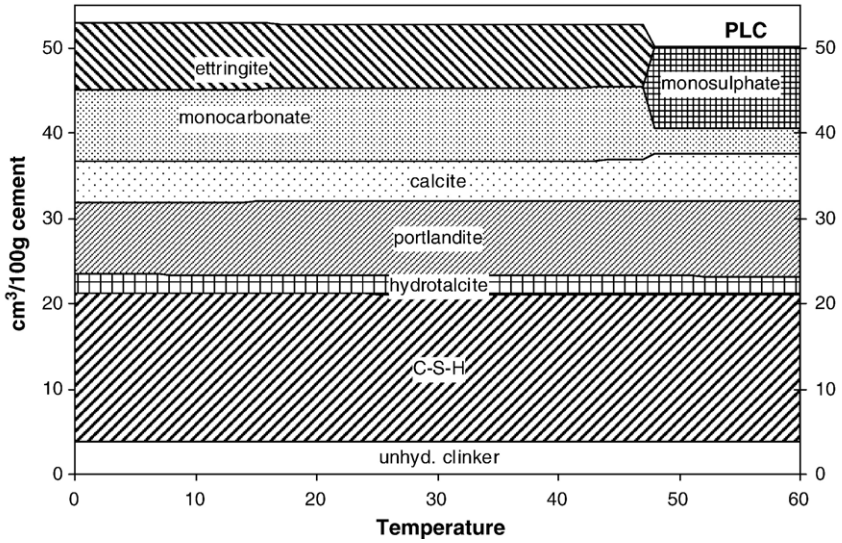

Fig. 6. Calculated volume of hydrates in PLC as a function of temperature assuming an equal dissolution of the clinker phases.

equilibrium modelling is a valid approach to describe mineralogical development during the course of hydration of Portland cements. The higher amount of monocarbonate is due to the surplus of Al in the PLC system, while the presence of more hydrotalcite is caused by the higher amount of magnesium present in PLC. The lower amount of portlandite and C–S–H is a result of the lower fraction of alite and belite present in PLC.

The calculations also indicate that the estimation of the degree of hydration by the amount of water incorporated in the hydrating cement (e.g. non-evaporable water content or the free water index [22]) is not an exact estimate of the degree of hydration as the amount of incorporated water depends strongly on the type and amount of hydrates formed as the hydrates differ greatly in water content. For example, the calculated amount of non-evaporable water in SRPC drops from 20.8 ml/100 g hydrated cement at 45 °C to 18.5 ml/100 g at 55 °C after a hydration time of 150 days. At and above 50 °C a hydrate assemblage with little or no ettringite is present and less water is incorporated which leads to an underestimation of the degree of hydration at higher temperatures if the degree of hydration is estimated from the amount of bound water.

4.4. Hydrates present above 50 °C

While it is possible to calculate the phase composition up to 100 °C, certain kinetic restrictions have been applied to the treatment of the thermodynamic data. The C–S–H phases are metastable with respect to crystalline phases such as jennite, tobermorite, or afwillite; at higher temperatures C–S–H can convert rapidly to crystalline phases. However, even at 85 °C, C–S–H had been found to be only partially crystallised [50,51] after prolonged equilibration times while its bulk solubility was still dominated by the C–S–H gel present [50,51], indicating that for C–S–H the approach here is valid up to above 80 °C.

The formation of siliceous hydrogarnets has been excluded in the present calculations as they form very slowly at room temperatures. At higher temperatures, however, their formation is much faster and it is probable that the formation of siliceous hydrogarnets has to be taken into account upon prolonged hydration at temperatures above 50 °C. For example, siliceous hydrogarnets have been observed in samples hydrated for 8 years at 85 °C [51]. The siliceous hydrogarnet includes much of the available sulphate in solid solution [51]. XRD and TGA measurements of SRPC and PLC hydrated at 80 °C for 28 and 150 days showed, besides some unhydrated clinkers, the presence of C–S–H, portlandite, hydrotalcite, calcite and siliceous hydrogarnet, while no AFt or AFm phase could be identified. Thus the calculations presented here are reliable indicators up to ~ 55 °C but prolonged hydration at higher temperatures favours formation of siliceous hydrogarnets, which also incorporate sulphate thereby reducing or even eliminating AFt and AFm phases.

4.5. Comparison between porosity and strength

The possibility of calculating the phase assemblage as a function of time also makes it possible to calculate the porosity of the respective cementitious material and to correlate calculated porosities with measured strength data. For comparison measured compressive strength data for mortar samples prepared from four different Portland-limestone cements and an ordinary Portland cement have been used [2,8].

Based on the calculated volumes of the hydrates, the unhydrated cements and the quartz aggregate used in the mortar experiments, the porosity as function of time and temperature was calculated according to

$$P_t = \frac{V_{\text{cement},t=0} + V_{\text{solution},t=0} - V_{\text{cement},t} - V_{\text{hydrates},t}}{V_{\text{cement},t=0} + V_{\text{solution},t=0} + V_{mortar}} \quad (7)$$

where P_t is the (total) porosity in %, V the volume in cm^3, $V_t=0$ is the volume before hydration, and V_t the volume at time t [52]. These calculations assume that no shrinkage occurs and the change in volume can therefore be expressed entirely in terms of porosity. Thus, the calculated "total" porosity corresponds to the difference between the initial volume of the system before the start of hydration and the volume of the hydrates, the unreacted cement plus pore solution at time t. This total porosity corresponds roughly to the sum of "gel" and "capillary" porosity but does not include the porosity created by air voids or cracks.

Comparison of calculated total porosity P_t with the measured strength data shows a good agreement (Fig. 7A). The relationship between the calculated porosity and the measured compressive strength f_c was fitted using $f_c=f_{c,0}\ (1-aP)$ [53], where $f_{c,0}$ is the hypothetical maximal compressive strength and a is a fitting constant. The calculated total porosity is slightly lower than the measured "total" porosity values. A weak dependence of the calculated total porosity on the temperature is observed in Fig. 7A.

Compressive strength is closely related to the capillary porosity (e.g. [54]). The fraction of capillary pores can be calculated from the total porosity by subtracting the volume of the gel pores [12,54]. If gel porosity is associated with C–S–H, the amount of gel pores can be calculated from the volume of the C–S–H present. The molecular volume of saturated C–S–H gel, nominally $C_{1.67}SH_4$, ([55], see also Appendix) is 103 cm^3/mol, 31 vol.% larger than the molecular volume (78 cm^3/mol) of $C_{1.7}SH_{2.1}$ (corresponding to C–S–H dried at 11% relative humidity; cf. [31,55]), resulting in a gel porosity factor of 0.31.

At higher temperatures where a denser inner product (IP) is formed [2,43,44], less gel porosity is present which would result in a higher capillary porosity at the same degree of hydration. Zhang [56] reported a 8% higher and 9% lower porosity for cements hydrated at 5 and 40 °C, respectively, than for cements hydrated at 20 °C. From these data, gel porosity factors of 0.43, 0.31, 0.25 and 0.20 were calculated for C–S–H following formation at 5, 20, 30 and 40 °C, respectively. The capillary porosities calculated by applying these gel porosity factors to the calculated volume of C–S–H show a good correlation with the measured compressive strength (Fig. 7B) and with measured capillary porosities [8]. The dependency of calculated porosity on temperature observed in Fig. 7A, is absent in Fig. 7B. A further increase of the quality of the fit could may be obtained

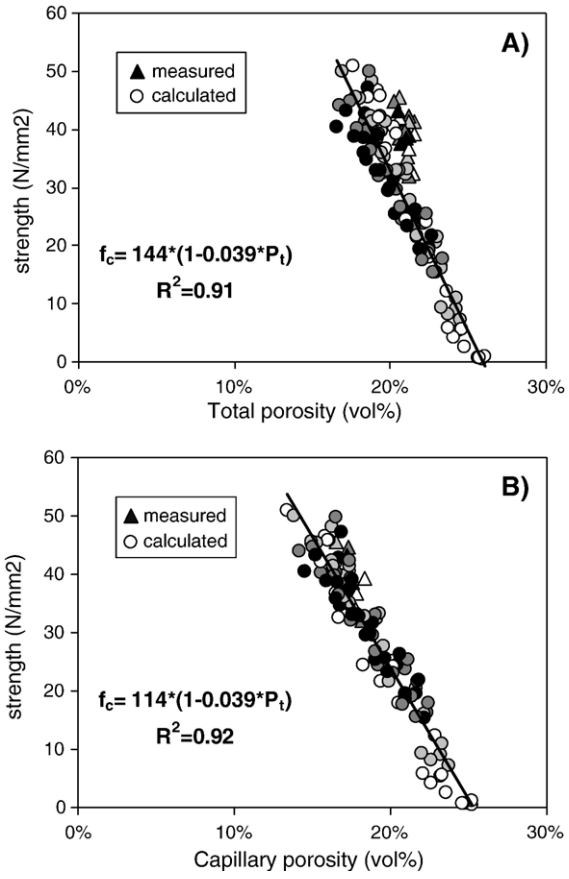

Fig. 7. Calculated A) total and B) capillary porosity of mortar samples compared to measured compressive strength. White data points indicate data from mortars hydrated at 5 °C, light grey refers to 20 °C, dark grey to 30 °C and black to 40 °C. Data for compressive strength and porosity (only 28 days values) are from Lothenbach et al. [2,8].

by considering the particle shape of the aggregate present in the mortars or by employing of a more detailed model to describe the dissolution of the clinkers.

The approach used in this paper to calculate the volume fraction and then the porosity is similar to the approach described by Parrot [12,52,57]. The main difference, however, is that the composition of the hydrate assemblage is not derived from a priori assumptions which solids are present but the hydrate assemblage is calculated directly from fundamental thermodynamic data. This allows for a greater flexibility (e.g. different hydrates might be present under different conditions) and extrapolations to different conditions.

5. Conclusions

The composition of the phase assemblage and the pore solution can be modelled with the model presented as a function of time and temperature. The results of thermodynamic modelling showed a good agreement with the experimental data. At both 5 and 20 °C, a similar phase assemblage is calculated to be present. The thermodynamic calculations predict the conversion of ettringite to monosulphate at approximately 50 °C, which agrees well with experimental observations in Portland cements [2,45]. It is also found that not only ettringite but also monocarbonate transforms to monosulphate at around 50 °C.

Modelling shows that in low-aluminium Portland cements with a molar $(Al,Fe)_2O_3/SO_3$ ratio <1 (<1.3 if expressed in bulk weight Al_2O_3/SO_3), at higher temperatures not only monosulphate but also small amounts of ettringite are expected to persist. In contrast, in Portland(-limestone) cements, with a molar $(Al,Fe)_2O_3/SO_3$ ratio >1, monocarbonate instead of ettringite is expected to be present above 50 °C.

The changes of the composition of the hydrate assemblage with increasing temperature decreases the volume of solids present in the hydrating cement, increases the porosity and thus influences negatively compressive strength. In addition to the conversion of ettringite and monocarbonate to monosulphate at and above 48 °C the densification of the C–S–H with increasing temperatures lead to further decreases of the volume of the solid phases.

A good correlation between calculated porosity and measured compressive strength was observed. A weak dependence of the calculated porosity on the temperature was observed, which disappeared when different densities of C–S–H at different temperatures were assumed. This indicates that other factors such as the heterogeneous distribution of the hydration products and differences in morphology of the hydrates (e.g. longer ettringite needles at lower temperature) play only a minor role for the strength development while the primary factor influencing strength is the degree of space filling or, conversely, the capillary porosity of the system as e.g. demonstrated by Verbeck and Helmuth [54].

Acknowledgments

The author thanks Frank Winnefeld (Empa), Josef Kaufmann (Empa), and Erich Wieland (PSI) for the stimulating discussions. Special thanks to Dmitrii Kulik (PSI) for his valuable help on how to master the many functions available in GEMS.

Appendix A

Thermodynamic modelling is carried out using the Gibbs free energy minimisation program GEMS [23]. For aqueous species as well as for many solids the Gibbs free energy of formation $\Delta_f G^\circ$, the enthalpy of formation $\Delta_f H^\circ$, the entropy S° and the heat capacity C_p° were taken from the PSI-GEMS thermodynamic dataset [24,25]. The Gibbs free energy of formation $\Delta_f G^\circ$ at 25 °C as given in Table 4 is related to the Gibbs free energy of reaction $\Delta_r G^\circ = \sum_i \nu_i \Delta_f G^\circ$ and to the solubility product $K_{S0} = e^{\frac{-\Delta_r G^\circ}{RT}}$, where ν_i are the stoichiometric reaction coefficients, R=8.31451 J/mol/K and T the temperature in K. Solubility products for cement minerals at 25 °C were taken from the compilation of Lothenbach and Winnefeld [6] completed with the data recently determined [27–29], resulting in the set of thermodynamic data for cements as given in Table 4: "cemdata2007". Activity coefficients of aqueous species γ_j are computed with the built-in extended Debye–Hückel equation in the Truesdell–Jones form with individual

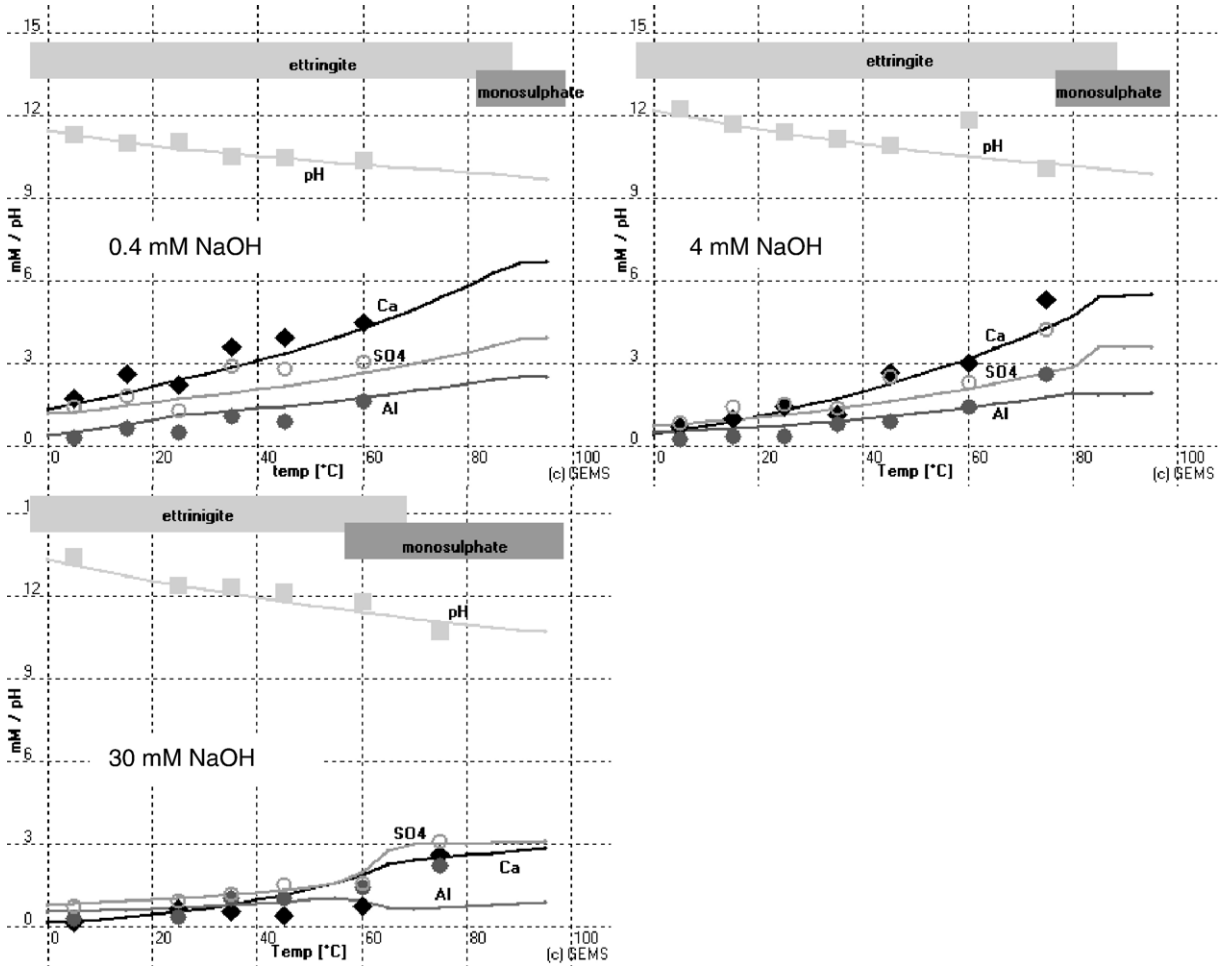

Fig. A.1. Comparison between measured data (dots) from Perkins and Palmer [47] and the calculated solubility (lines) of (Al-)ettringite using the thermodynamic data given in Table 4.

parameters a_γ° (as given in [25]) and a common third parameter b_γ of 0.064:

$$\log\gamma_j = \frac{-A_\gamma z_j^2\sqrt{I}}{1+B_\gamma a_\gamma^0\sqrt{I}} + b_\gamma I$$

where z_j denotes the charge of species j, I the effective molal ionic strength and A_γ and B_γ are P,T-dependent coefficients [23].

The thermodynamic data between 0 and 100 °C were calculated using the temperature dependence of the apparent Gibbs free energy of formation $\Delta_a G^\circ$ according to Eq. (6). The entropy S° and the enthalpy of formation $\Delta_f H^\circ$ were fitted from experimental solubility data from literature or estimated, if no experimental data were available (see below). Where available, measured heat capacities C_p° were used. In cases where they were missing they were estimated from the heat capacity of other structural similar solids assuming $\Delta_r C_p^\circ = 0$ for reactions involving only solids. Similar, for the few cases where no temperature dependent solubility data were available, the entropy of the solid was estimated assuming $\Delta_r S^\circ = 0$ from other structural similar solids. The $\Delta_r S^\circ = 0$ and $\Delta_r C_p^\circ = 0$ assumption is reasonable (cf. [41,42,58]) and the results are in many cases very good if only solids are involved in the formulated reactions. Molecular volumes V° at standard conditions were calculated from the volume of the crystallographic unit cell or from densities derived from crystallographic data. In many cases the data compiled in Taylor [31] were used.

A.1. AFt

Solubility measurements of (Al-)ettringite ($C_6A\,\overline{S}_3H_{32}$)[2] at temperatures from 5 to 85 °C have been published [47,48,59–61]. Based on the experimental data at 25 °C of Perkins and Palmer [47] and Warren and Reardon [60] a solubility product of $10^{-44.9\pm0.7}$ was calculated for the reaction $Ca_6Al_2(SO_4)_3(OH)_{12}\cdot 26H_2O(s) \Leftrightarrow 6Ca^{2+} + 2Al(OH)_4^- + 3SO_4^{2-} + 4OH^- + 26H_2O$. Using the data measured between 5 and 75 °C [47] (Fig. A.1) and the heat capacity as measured by Ederova and Satava [30] (cf. Table 4), an enthalpy of formation $\Delta_f H^\circ$ of − 17535 kJ/mol and entropy S° of 1900 J/K/mol was fitted.

[2] Cement short-hand notation is used: A=Al_2O_3; C=CaO; $\overline{C}$=CO_2; F=Fe_2O_3; H=H_2O; S=SiO_2; $\overline{S}$=SO_3; C–S–H=(non-stoichiometric) calcium silicate hydrate.

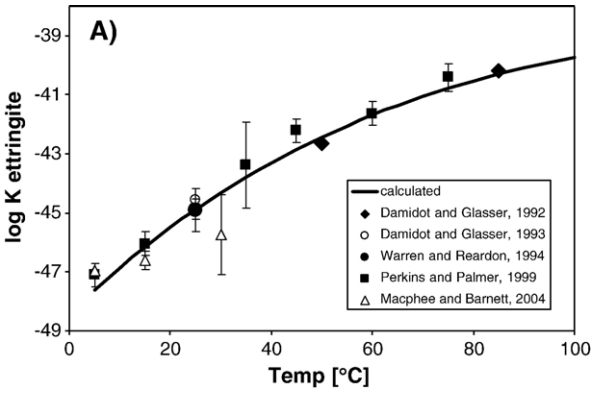

Fig. A.2. Comparison between calculated solubility product of ettringite as a function of temperature with literature data. Solubility products for Warren and Reardon [60], Perkins and Palmer [47] and Macphee and Barnett [59] were recalculated based on the reported concentrations, solubility products of Damidot and Glasser [48,61] were given as reported.

Measured values of the enthalpy of formation $\Delta_f H°$ (−17548 kJ/mol (4194 kcal/mol) [62] and −17493 kJ/mol [63]) are in good agreement with the fitted value. The log K values calculated (−47.62 at 5, −46.16 at 15, −44.90 at 25, −43.80 at 35, −42.86 at 45, −41.69 at 60, −40.81 at 75 and −40.30 at 85 °C) compare well with different data reported in the literature data (Fig. A.2).

The temperature at which ettringite transforms to monosulphoaluminate depends strongly on the availability of sulphate and on the hydroxide concentration. Calculations, based on the experiments of Perkins and Palmer [47], see Fig. A.1, show that at a hydroxide concentration of 1 mmol/l, which corresponds at 20 °C to a pH of approximately 10.9, this transformation occurs at approximately 90 °C, at a hydroxide concentration of 10 mmol/l (pH 12.0 at 20 °C) at 70 °C and at a hydroxide concentration of 100 mmol/l (pH 13.1 at 20 °C) at 50 °C. In cement systems, the situation is more complex and the availability of sulphate and aluminium play also an important role (cf. Figs. 5 and 6).

Tricarboaluminate ($Ca_6Al_2(CO_3)_3(OH)_{12}\cdot 26H_2O$), a structural carbonate analogue of ettringite, is unstable relative to calcium monocarboaluminate [64]. Pöllmann and Kuzel [65] and Matschei et al. [27] reported the extensive (but not complete) formation of solid solutions between the sulphate and carbonate ettringite end-members. The sulphate containing ettringite is more stable than the CO_3-substituted ettringites. The solubility product of tricarboaluminate ($C_6A\bar{C}_3H_{32}$) has been recently determined by Matschei et al. [27] as $10^{-46.5}$ at 25 °C. Solubility data at other temperatures are not available, thus entropy and heat capacity were estimated assuming $\Delta_r S°=0$ and $\Delta_r C_p°=0$ for the reaction: $3CaO\cdot Al_2O_3\cdot 3CaSO_4\cdot 32H_2O(s)+3CaCO_3(s)\Leftrightarrow 3CaO\cdot Al_2O_3\cdot 3CaCO_3\cdot 32H_2O(s)+3CaSO_4(s)$ resulting in $S°=1858$ and $C_p°=2121$ J/K/mol at 25 °C (see Table 4).

Up to about 42 mol% of the sulphate in the ettringite may be replaced by carbonate, while only up to 4% of the carbonate of the tricarboaluminate end member can be replaced by sulphate [27]. This solid solution was modelled using the non-regular Redlich–Kistler expression to calculate the activity of the solid phase (cf. [66,67]) using the dimensionless coefficients $a_0=-0.823$ and $a_1=2.82$ [27].

Thaumasite $(CaSiO_3)_2(CaSO_4)_2(CaCO_3)_2\cdot 30H_2O$ has a structure similar to ettringite and is reported to form limited solid solution with ettringites. The solubility of synthetic thaumasite intermixed with ettringite has been measured by Macphee and Barnett [59], a significantly lower solubility has been measured for thaumasite from a geological source [68]. No thermodynamic data are selected in this paper due to the lack of reliable data measured in pure systems.

A.2. Hydrogarnet

Matschei et al. [27] derived from solubility measurements of hydrogarnet (C_3AH_6) at temperatures from 5 to 105 °C together with critically reviewed data from the literature a solubility product of $10^{-20.84}$ for the reaction $Ca_3Al_2(OH)_{12}(s)\Leftrightarrow 3Ca^{2+}\ 2Al(OH)_4^-+4OH^-$ (cf. Table 4). The derived enthalpy of formation $\Delta_f H°$ of −5540 kJ/mol is similar to the value of −5548 kJ/mol derived by Babushkin et al. [40] and to the experimentally determined values of −5561 kJ/mol and −5552 kJ/mol [62,69]. Also for hydrothermally synthesised siliceous hydrogarnet ($C_3AS_{0.8}H_{4.4}$) thermodynamic data have been measured [27], cf. Table 4. Even though siliceous hydrogarnet is thermodynamically stable at 20 °C, its formation at room temperature is very slow and thus its formation is not considered in the present calculations. However, the formation of siliceous hydrogarnets has been observed in cement samples aged for 9 years and more [7] and in cements hydrated at higher temperature(e.g. [51]).

A.3. AFm

The AFm phases ($C_4(A,F)X_2\cdot yH_2O$, where X denotes one formula unit of a single charged anion) occurring in cements are mineralogically and chemically complex. Its layer structure incorporates variable amounts of water as well as anions such as hydroxyl, sulphate, silicon, aluminate, or carbonate.

At room temperature the metastable phases C_2AH_8 and C_4AH_{13} can persist for a long time in contact with aqueous solutions; they convert only slowly to the stable C_3AH_6. At 50 °C, however, they start to convert to hydrogarnet within hours or days [70]. A number of solubility data in the range from 1 to 50 °C [70–77] have been reported. These data in the temperature range 1–50 °C are reproduced well using an entropy $S°$ of 440±10 (C_2AH_8) and 700±20 J/K/mol (C_4AH_{13}) and the corresponding enthalpies of formation $\Delta_f H°$ calculated from $\Delta_f G°$ and $S°$ (see Fig. A.3 and Table 4). The fitted data agree well with the entropies given by Babushkin et al. [40] of 445 and 718 J/K/mol, respectively. Also the calculated $\Delta_f H°$ of −5432 and −8302 kJ/mol agree well with the data reported by Babushkin et al. [40] of −5436 and −8318 kJ/mol.

The heat capacity of C_4AH_{13} and C_2AH_8 (Table 4) was estimated assuming $\Delta_r C_p°=0$ for the reactions: $3CaO\cdot Al_2O_3\cdot CaSO_4\cdot 12H2O(s)+Ca(OH)_2(s)\Leftrightarrow 3CaO\cdot Al_2O_3\cdot Ca(OH)_2\cdot 12H_2O(s)+CaSO_4(s)$ and $0.5[3CaO\cdot Al_2O_3\cdot Ca(OH)_2\cdot 12H_2O(s)]+Al(OH)_3(s)\Leftrightarrow 2CaO\cdot Al_2O_3\cdot 8H_2O(s)$.

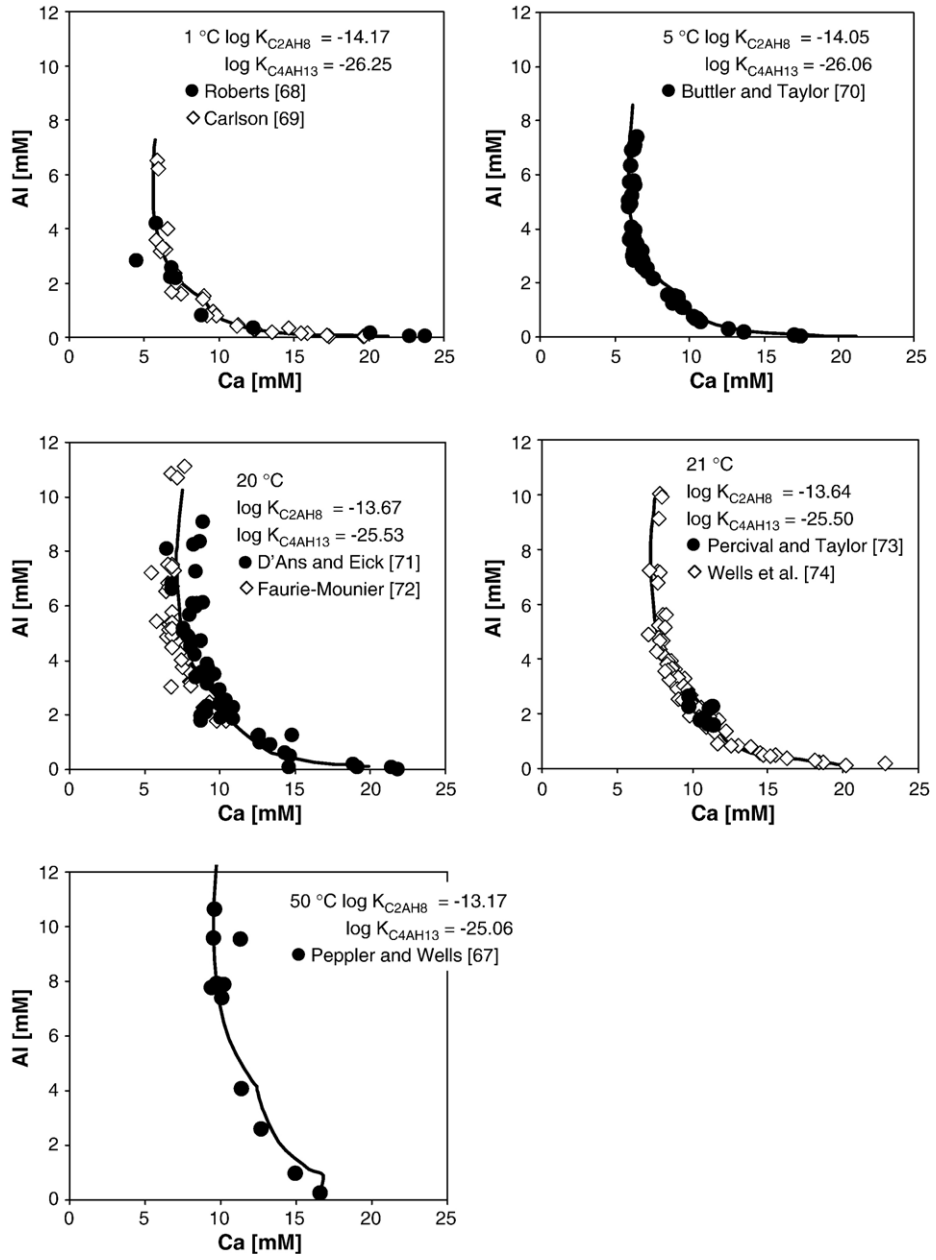

Fig. A.3. Comparison between measured literature data [70–77] and the calculated solubility (lines) of C_2AH_8 and C_4AH_{13} using the thermodynamic data given in Table 4.

The thermodynamic data for monosulphoaluminate ($3CaO{\cdot}Al_2O_3{\cdot}CaSO_4{\cdot}12H_2O$), monocarboaluminate ($CaO{\cdot}Al_2O_3{\cdot}CaCO_3{\cdot}11H_2O$), hemicarboaluminate ($Ca_4Al_2O_{6.5}(CO_3)_{0.5}{\cdot}12H_2O$) and stratlingite ($2CaO{\cdot}Al_2O_3{\cdot}SiO_2{\cdot}8H_2O$) between 5 and 85 °C have been recently determined [27,28]. The corresponding data in Table 4 are taken directly from Matschei et al. [27], who used the same set of auxiliary data. The calculated enthalpies of formation of −8750 kJ/mol (monosulphoaluminate) and −8250 kJ/mol (monocarboaluminate) [27] are slightly higher than the values measured by Berman and Newman [78] of −8786 kJ/mol and −8280 kJ/mol and Babushkin et al. [40]: −8772 kJ/mol (− 2096.44 kcal/mol) and −8207 kJ/mol (−1961.6 kcal/mol), respectively.

The heat capacity $C_p°$ of monosulphoaluminate has been measured by Ederova and Satava [30]; $C_p°$ values for monocarboaluminate, hemicarboaluminate and stratlingite are estimated assuming $\Delta_r C_p° = 0$ [41,58] for the following reactions: $3CaO{\cdot}Al_2O_3{\cdot}CaSO_4{\cdot}12H_2O(s) + CaCO_3(s) \Leftrightarrow 3CaO{\cdot}Al_2O_3{\cdot}CaCO_3 11H_2O(s) + 0.5CaSO_3(s) + 0.5CaSO_3{\cdot}2H_2O(s)$, $0.5[3CaO{\cdot}Al_2O_3{\cdot}CaCO_3{\cdot}11H_2O(s)] + 0.5[3CaO{\cdot}Al_2O_3{\cdot}(Ca(OH)_2){\cdot}12H_2O(s)] \Leftrightarrow 3CaO{\cdot}Al_2O_3(Ca(OH)_2)_{0.5}(CaCO_3)_{0.5}11.5H_2O(s)$, and $2CaO{\cdot}Al_2O_3{\cdot}8H_2O(s) + SiO_2(s) \Leftrightarrow 2CaO{\cdot}Al_2O_3{\cdot}SiO_2{\cdot}8H_2O$ (stratlingite). The resulting data are compiled in Table 4.

AFm phases have essentially fixed compositions, with exception of the limited solid solution between C_4AH_x and monosulphoaluminate [28,79,80]. Up to about 50 mol% of the

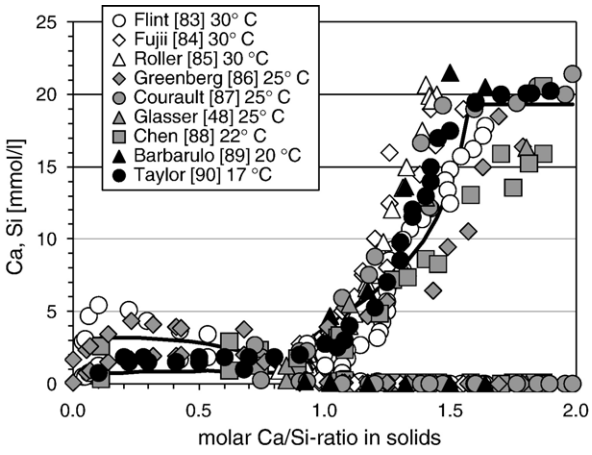

Fig. A.4. Comparison between literature data [50,86–93] measured between 17 and 30 °C and the calculated solubility (lines) at 25 °C of C–S–H using the thermodynamic data given in Table 4.

sulphate in the monosulphoaluminate may be replaced by OH^-, while less than 3% of the OH^- of the C_4AH_x-endmember can be replaced by sulphate [28]. Thus, no solid solution formation has been considered between the AFm phases, with exception of C_4AH_x and monosulphoaluminate. This solid solution was modelled using the non-regular Redlich–Kistler expression using the dimensionless coefficients $a_0=0.188$ and $a_1=2.49$ [27].

A.4. Hydrotalcite

MgO present in the clinker phases will dissolve in the presence of water and precipitate in cementitious systems as brucite ($Mg(OH)_2$) or as hydrotalcite, depending on the chemical conditions. Hydrotalcites have a variable composition of the general formula $Mg_{1-x}(Al,Fe)_x(OH)_2\cdot[A^{n-}]_{x/n}\cdot mH_2O$, and a structure composed of positively charged brucite like layers intercalated with anions $[A^{n-}]$ and water molecules. The structure can accommodate a number of cations including Mn, Mg, Ni, Zn, Al, Fe, interlayer anions such as OH^-, Cl^-, CO_3^{2-} and SO_4^{2-} and varying amount of water. For OH-hydrotalcite ($Mg_4Al_2(OH)_{14}\cdot 3H_2O(s)$) a solubility product of $10^{-56.02}$ and for CO_3-hydrotalcite ($Mg_4Al_2(OH)_{12}\,CO_3\cdot 3H_2O(s)$) a solubility product of $10^{-51.14}$ has been determined [6]. These thermodynamic data indicate that under conditions typical for Portland cements, i.e. a low partial pressure of CO_2, OH-hydrotalcite is more stable than CO_3-hydrotalcite.

The entropy and the heat capacity of hydrotalcite were calculated from the data given by Allada et al. [81] for $Mg_{5.69}Al_2(OH)_{15.38}\cdot CO_3\cdot 3H_2O(s)$ ($S°=658.31\pm0.17$ J/K/mol, $C_p°=777$ J/K/mol). The heat capacities values measured by Allada et al. [81] between 0 and 310 K can be described by $C_p=-211.40+4.27*T-2296*T^{-2}+628.97*T^{-0.5}-0.00424*T^2+2.11E-6*T^3$. The enthalpy and heat capacity values were then calculated based on the data given in Table 4 using $\Delta_r S°=0$ and $\Delta_r C_p°=0$ for: $Mg_{5.69}Al_2(OH)_{15.38}\cdot CO_3\cdot 3H_2O(s)\Leftrightarrow Mg_4Al_2(OH)_{14}\cdot 3H_2O(s)+0.69Mg(OH)_2(s)+1MgCO_3(s)$ $Mg_{5.69}Al_2(OH)_{15.38}\cdot CO_3\cdot 3H_2O(s)\Leftrightarrow Mg_4Al_2(OH)_{12}\,CO_3\cdot 3H_2O(s)+1.69Mg(OH)_2(s)$ resulting in $C_p=-363.9+4.208*T+3.754e6*T^{-2}+628.97*T^{-0.5}-0.00424*T^2+2.11E-6*T^3$ for $Mg_4Al_2(OH)_{14}\cdot 3H_2O(s)$ and $C_p=-382.4+4.244*T+4.324e6*T^{-2}+628.97*T^{-0.5}-0.00424*T^2+2.11E-6*T^3$ for $Mg_4Al_2(OH)_{12}\,CO_3\cdot 3H_2O(s)$.

A.5. Fe-hydrates

Fe-ettringite ($Ca_6Fe_2(SO_4)_3(OH)_{12}\cdot 26H_2O$) is a structural analogue of ettringite which forms a solid solution with the Al-bearing ettringite [31,82]. Its solubility product has been recently determined by Möschner et al. [29] as $10^{-44.0\pm0.7}$ for the reaction $Ca_6Fe_2(SO_4)_3(OH)_{12}\cdot 26H_2O(s)\Leftrightarrow 6Ca^{2+}+2Fe(OH)_4^-+3SO_4^{2-}+4OH^-+26H_2O$. Fe-ettringite has thus $10^{-0.9}$ times higher solubility product than (Al-)ettringite with $10^{-44.9}$.

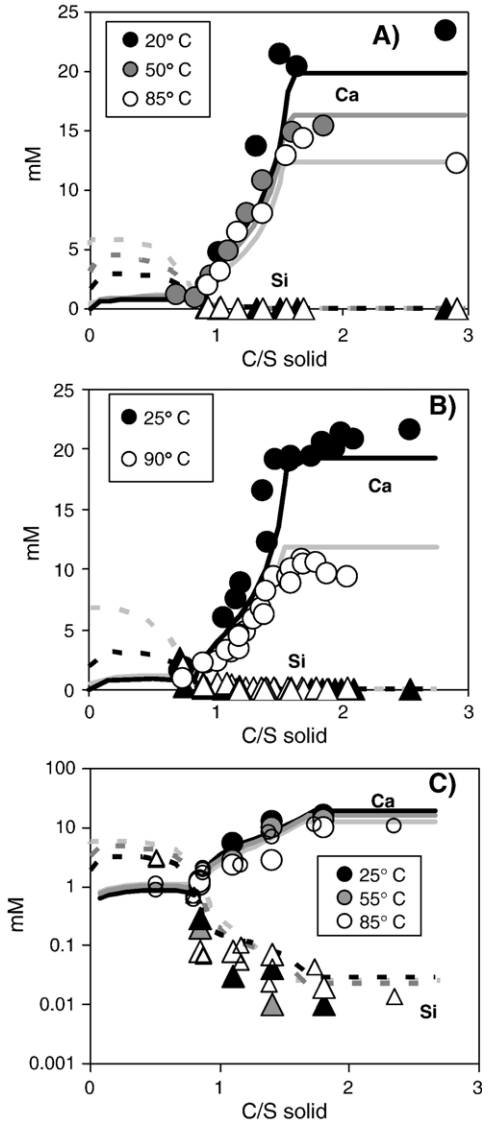

Fig. A.5. A) Measured (symbols: Barbarulo [92]) and calculated solubility (lines) of C–S–H at 20, 50 and 85 °C B) Measured (symbols: data from Courault [90]) and calculated solubility (lines) of C–S–H at 25 and 90 °C. C) Measured (big symbols: Glasser et al. [50]; small symbols: Atkins et al. [95]) and calculated solubility (lines) of C–S–H at 25, 55 and 85 °C.

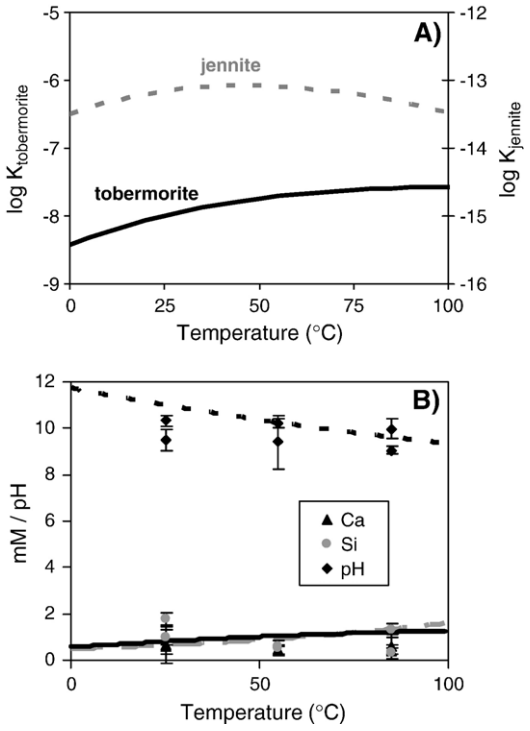

Fig. A.6. A) Calculated changes of the solubility products of tobermorite and jennite as a function of temperature. B) Measured (dots: Dickson et al. [96]) and calculated solubility (lines) of tobermorite in H_2O using the thermodynamic data given in Table 4.

No experimentally derived solubility data for Fe-hydrogarnet (C_3FH_6) are available in the literature. Babushkin et al. [40] estimated between ferric and aluminium hydrates a constant difference in standard enthalpy and entropy of −215.2 kcal/mol and 4.8 cal/mol/K, respectively. This approach was applied to calculate the Gibbs free energies and the solubility product of Fe-hydrogarnet resulting in solubility product of $10^{-25.16}$ for the reaction $Ca_3Fe_2(OH)_{12}(s) \Leftrightarrow 3Ca^{2+} + 2Fe(OH)_4^- + 4OH^-$ (cf. Table 4), a solubility product which is $10^{-4.32}$ times lower than the solubility product of C_3AH_6 ($10^{-20.84}$).

The solubility of Fe-monosulphate ($3CaO{\cdot}Fe_2O_3{\cdot}CaSO_4{\cdot}12H_2O$) and Fe-monocarbonate ($CaO{\cdot}Al_2O_3{\cdot}CaCO_3{\cdot}12H_2O$) has been measured [29] and the corresponding solubility products at 25 °C are $10^{-33.2\pm0.5}$ and $10^{-35.5\pm0.3}$. These solubility products are approximately $10^{-4.0}$ times lower than the solubility products of their Al-containing analogues ($10^{-29.3}$ and $10^{-31.5}$). This value agrees well with estimation of Babushkin et al. [40] of $10^{-4.3}$, see above. Thus, the solubility products for the other Fe-containing AFm phases: Fe-hemicarbonate($Ca_4Fe_2O_{6.5}(CO_3)_{0.5}{\cdot}11.5H_2O$), Fe-stratlingite ($2CaO{\cdot}Fe_2O_3{\cdot}SiO_2{\cdot}8H_2O$), C_4FH_{13} and C_2FH_8 and for Fe-hydrotalcite are estimated from their Al-analogues using a $10^{-4.0}$ times lower solubility product.

The entropy and heat capacity data needed to extrapolate these data to other temperatures were estimated assuming $\Delta_r S° = 0$ and $\Delta_r C_p° = 0$ for the reaction: Al-hydrate + Fe_2O_3 (hematite) ⇔ Fe-hydrate + Al_2O_3(corundum) and are given in Table 4. It should be noted that some of the thermodynamic data for Fe-hydrates are not derived from experimental data and thus should be considered as rough estimates only. For modelling, the presence of ideal solid solutions between the Fe-hydrates and its respective Al-analogues are assumed (cf. [83]) with exception of ettringite, where the presence of a miscibility gap from $0.25 \le Al/(Fe+Al) \le 0.65$ has been described [84]. The solid solution between $Ca_3Fe(SO_4)_{1.5}(OH)_6{\cdot}13H_2O(s)$ and $Ca_3Al(SO_4)_{1.5}(OH)_6{\cdot}13H_2O(s)$ was modelled using the dimensionless coefficients $a_0 = 2.1$ and $a_1 = -0.169$ [84].

The expressions ettringite, monocarbonate, monosulphate, hemicarbonate or hydrotalcite in this paper all refer to the solid solution between the Al- and Fe-containing analogues.

A.6. C–S–H

C–S–H phases are modelled using the solid solution model developed by Kulik and Kersten [38,85], where the C–S–H system is described as a system of two concurrent ideal solid solution systems:

i) CSH-I solid solution system with the end-members SiO_2 (am) and tobermorite (Tob-I: $(CaO)_2(SiO_2)_{2.4}{\cdot}(H_2O)_{3.2}$) and
ii) CSH-II solid solution system with the end-members jennite $(CaO)_{1.67}(SiO_2)_1{\cdot}(H_2O)_{2.1}$ and tobermorite (Tob-II: $(CaO)_{0.83}(SiO_2)_1{\cdot}(H_2O)_{1.3}$).

Solubility products for the solids were refitted using the solid solution model described above and experimental data from different sources [50,86–93] (see Fig. A.4). The calculated log K values for jennite $(CaO)_{1.67}(SiO_2)(H_2O)_{2.1}$ is with −13.17 the same as obtained before [6], while the value of tobermorite $(CaO)_{0.83}(SiO_2)(H_2O)_{1.3}$ is with −8.0 slightly lower. Both values agree well with the solubility products (−13.4 and −8.33, respectively) calculated by Kulik and Kersten [85]. In contrast to earlier calculations [6,7,38,85], slightly less water was assumed to be present per C–S–H and the Gibbs free energies were corrected accordingly. The molar volume (78 cm^3/mol) of jennite ($C_{1.67}SH_{2.1}$) was calculated from the molecular weight and a density of 2.44 kg/dm^3 [31,55]. The molar volume of a saturated C–S–H gel $C_{1.67}SH_4$ (density 2.195 kg/dm^3 [55]) is with 103 cm^3/mol 31 vol.% larger. A molar volume of 59 cm^3/mol was calculated for 14 Å-tobermorite ($C_{0.83}SH_{1.33}$) from density data (2.23 kg/dm^3 [94]).

Solubility measurements of C–S–H at a C/S > 1 show at higher temperatures lower Ca concentrations and equal or higher Si concentrations [50,90,92,95]. These measured Ca and Si concentrations at 50, 85 and 90 °C [50,90,92,95] are used to estimate the enthalpy of formation $\Delta_f H°$ and entropy $S°$ of jennite and tobermorite. These $S°$ values are with 140 and 80 J/mol/K somewhat lower then the $S°$ estimated from the data given by Babushkin et al. [40] (jennite 187 J/mol/K, tobermorite 118 J/mol/K). Even though the estimated $S°$ values are not accurate (±50 J/mol/K), this uncertainty introduces less than 0.5 log K_{S0} error below 100 °C and gives a good estimate of the trends of C–S–H solubility at different temperatures (Fig. A.5). The calculated solubility products of tobermorite and jennite do not change very much between 0 and 100 °C, which is consistent with the data

measured by Dickson et al. [96] for a number of different C–S–H phases (Fig. A.6). It should be noted that C–S–H is metastable with respect to crystalline phases but this condition is suspended in the calculations to conform the observations. Nevertheless, C–S–H does show instability towards the higher range of temperatures included in this study, particularly if free water is present to facilitate crystallization.

Standard values of the heat capacity were estimated using the additivity principle ($\Delta_r C_p^\circ = 0$) from the respective values of $(CaO)_3(SiO_2)_2(H_2O)_3$ (afwillite), $(CaO)_5(SiO_2)_6(H_2O)_{5.5}$ (tobermorite) $(CaO)_5(SiO_2)_6(H_2O)_{10.5}$ (plombierite), and $Ca(OH)_2$ (portlandite) (cf. [38]). Heat capacities for afwillite, tobermorite and plombierite were taken from Babushkin et al. [40], who predicted C_p° values for a number of hydrated calcium silicates; values for $Ca(OH)_2$ were taken from Table 4.

References

[1] J.I. Escalante-Garcia, J.H. Sharp, Effect of temperature on the hydration of the main clinker phases in Portland cements: Part I, neat cements, Cem. Concr. Res. 28 (9) (1998) 1245–1257.

[2] B. Lothenbach, F. Winnefeld, C. Alder, E. Wieland, P. Lunk, Effect of temperature on the pore solution, microstructure and hydration products of Portland cement pastes, Cem. Concr. Res. 37 (4) (2007) 483–491.

[3] W.H. Price, Factors influencing concrete strength, J. Am. Conc. Inst. 47 (31) (1951) 417–432.

[4] K.O. Kjellsen, R.J. Detwiler, O.E. Gjorv, Development of microstructures in plain cement pastes hydrated at different temperatures, Cem. Concr. Res. 21 (1) (1991) 179–189.

[5] J.J. Thomas, D. Rothstein, H.M. Jennings, B.J. Christensen, Effect of hydration temperature on the solubility behavior of Ca-, S-, Al-, and Si-bearing solid phases in Portland cement pastes, Cem. Concr. Res. 33 (12) (2003) 2037–2047.

[6] B. Lothenbach, F. Winnefeld, Thermodynamic modelling of the hydration of Portland cement, Cem. Concr. Res. 36 (2) (2006) 209–226.

[7] B. Lothenbach, E. Wieland, A thermodynamic approach to the hydration of sulphate-resisting Portland cement, Waste Manage. 26 (7) (2006) 706–719.

[8] B. Lothenbach, C. Alder, F. Winnefeld, P. Lunk, Einfluss der Temperatur und Lagerungsbedingungen auf die Festigkeitsentwicklung von Mörteln und Betonen, Beton 55 (12) (2005) 604–609.

[9] SN 505 262/1, Betonbauten: Materialprüfung, Schweizer Ingenieur-und Architektenverein, Zürich, 2003.

[10] S.-Y. Hong, F.P. Glasser, Alkali binding in cement pastes. Part I. The C–S–H phase, Cem. Concr. Res. 29 (1999) 1893–1903.

[11] J.A. Dalziel, W.A. Gutteridge, The influence of pulverized-fuel ash upon the hydration characteristics and certain physical properties of a Portland cement paste, Cement and Concrete Association, Slough, 1986.

[12] L.J. Parrot, Modeling of hydration reactions and concrete properties, in: J.P. Skalny (Ed.), Materials Science of Concrete, Westerville, OH, 1989, pp. 181–195.

[13] T. Kishi, K. Maekawa, Multi-component model for hydration heating of Portland cement, Conc. Lib. JSCE 28 (1996) 97–115.

[14] H.F.W. Taylor, A method for predicting alkali ion concentrations in cement pore solutions, Adv. Cem. Res. 1 (1) (1987) 5–17.

[15] J.K. Kim, S.H. Han, K.M. Lee, Estimation of compressive strength by a new apparent activation energy function, Cem. Concr. Res. 31 (2001) 217–225.

[16] P. Lawrence, M. Cyr, E. Ringot, Mineral admixtures in mortars. Effect of inert materials on short-term hydration, Cem. Concr. Res. 33 (2003) 1939–1947.

[17] F. Ridi, E. Fratini, F. Manelli, P. Baglioni, Hydration process of cement in the presence of a cellulosic additive. A calorimetric investigation, J. Phys. Chem., B 109 (2005) 14727–14734.

[18] K.O. Kjellsen, R.J. Detwiler, Reaction-kinetics of Portland-cement mortars hydrated at different temperatures, Cem. Concr. Res. 22 (1) (1992) 112–120.

[19] L.E. Copeland, D.L. Kantro, Hydration of Portland cement, Proc 5th International Congress on the Chemistry of Cement, Tokyo, 1968, pp. 387–420.

[20] L. D'Aloia, G. Chanvillard, Determining the "apparent" activation energy of concrete Ea-numerical simulations of the heat of hydration of cement, Cem. Concr. Res. 32 (2002) 1277–1289.

[21] S. Swaddiwudhipong, D. Chen, M.H. Zhang, Simulation of the exothermic process of Portland cement, Adv. Cem. Res. 14 (2) (2002) 61–69.

[22] A. Damasceni, L. Dei, E. Fratini, F. Ridi, S.H. Chen, P. Baglioni, A novel approach based on differential scanning calorimetry applied to the study of tricalcium silicate hydration kinetics, J. Phys. Chem., B 106 (2002) 11572–11578.

[23] D. Kulik, GEMS-PSI 2.1, PSI-Villigen, Switzerland, 2005 available at http://les.web.psi.ch/Software/GEMS-PSI/.

[24] T. Thoenen, D. Kulik, Nagra/PSI chemical thermodynamic database 01/01 for the GEM-Selektor (V.2-PSI) geochemical modeling code, PSI, Villigenavailable at, http://les.web.psi.ch/Software/GEMS-PSI/doc/pdf/TM-44-03-04-web.pdf. 2003.

[25] W. Hummel, U. Berner, E. Curti, F.J. Pearson, T. Thoenen, Nagra/PSI Chemical Thermodynamic Data Base 01/01, Universal Publishers/uPUBLISH.com, USA, also published as Nagra Technical Report NTB 02-16, Wettingen, Switzerland, 2002.

[26] J.W. Johnson, E.H. Oelkers, H.C. Helgeson, SUPCRT92: a software package for calculating the standard molal thermodynamic properties of minerals, gases, aqueous species, and reactions from 1 to 5000 bar and 0 to 1000 °C, Comput. Geosci. 18 (7) (1992) 899–947.

[27] T. Matschei, B. Lothenbach, F.P. Glasser, Thermodynamic properties of Portland cement hydrates in the system $CaO–Al_2O_3–SiO_2–CaSO_4–CaCO_3–H_2O$, Cem. Concr. Res. in press.

[28] T. Matschei, B. Lothenbach, F.P. Glasser, The AFm phase in Portland cement, Cem. Concr. Res. 37 (2) (2007) 118–130.

[29] G. Möschner, B. Lothenbach, J. Rose, A. Ulrich, R. Figi, R. Kretschmar, Solubility of Fe-ettringite (Ca6[Fe(OH)6]2(SO4) ·26H O), Geochim Cosmochim Acta (in press).

[30] J. Ederova, V. Satava, Heat capacities of C_3AH_6, C_4ASH_{12} and $C_6AS_3H_{32}$, Thermochim. Acta 31 (1979) 126–128.

[31] H.F.W. Taylor, Cement Chemistry, Thomas Telford Publishing, London, 1997.

[32] H.F. McMurdie, M.C. Morris, E.H. Evans, B. Paretzkin, W. Wong-Ng, Y. Zhang, Standard X-ray diffraction powder patterns the JCPDS research associateship, Powder Diffr. 2 (1) (1987) 41–52.

[33] M. Ecker, H. Pöllmann, Powder Diffraction File for $3CaO·Fe_2O_3·CaSO_4·12H_2O$, PDF 00-041-1472, 1991.

[34] H. Pöllmann, M. Ecker, Powder Diffraction File for $3CaO·Fe_2O_3·CaCO_3·12H_2O$, PDF 00-043-0480, 1992.

[35] G. Mascolo, O. Marino, A new synthesis and characterization of magnesium–aluminium hydroxides, Mineral. Mag. 43 (1980) 619–621.

[36] M. Bellotto, B. Rebours, O. Clause, J. Lynch, D. Bazin, E. Elkaim, A reexamination of hydrotalcite crystal chemistry, J. Phys. Chem. 100 (20) (1996) 8527–8534.

[37] T. Sato, H. Fujita, T. Endo, M. Shimada, Synthesis of hydrotalcite-like compounds and their physico-chemical properties, React. Solids 5 (1988) 219–228.

[38] D.A. Kulik, M. Kersten, Aqueous solubility diagrams for cementitious waste stabilization systems: II, End-member stoichiometries of ideal calcium silicates hydrate solid solutions, J. Am. Ceram. Soc. 84 (12) (2001) 3017–3026.

[39] H.C. Helgeson, J.M. Delany, H.W. Nesbitt, D.K. Bird, Summary and critique of the thermodynamic properties of rock-forming minerals, Am. J. Sci. 278-A (1978) 1–229.

[40] V.I. Babushkin, G.M. Matveyev, O.P. Mchedlov-Petrossyan, Thermodynamics of Silicates, Springer–Verlag, Berlin, 1985.

[41] G.M. Anderson, D.A. Crerar, Thermodynamics in Geochemistry: the Equilibrium Model, Oxford University Press, Oxford, 1993.

[42] D. Kulik, Minimising uncertainty induced by temperature extrapolations of thermodynamic data: a pragmatic view on the integration of

thermodynamic databases into geochemical computer codes, Proc The use of thermodynamic databases in performance assessment, Barcelona, OECD, 2002, pp. 125–137.
[43] K.O. Kjellsen, H.M. Jennings, Observations of microcracking in cement paste upon drying and rewetting by environmental scanning electron microscopy, Adv. Cem. Based Mater. 3 (1996) 14–19.
[44] C. Famy, K.L. Scrivener, A.K. Crumbie, What causes differences of C–S–H gel grey levels in backscattered electron images? Cem. Concr. Res. 32 (9) (2002) 1465–1471.
[45] A.N. Christensen, T.R. Jensen, J.C. Hanson, Formation of ettringite, $Ca_6Al_2(SO_4)_3(OH)_{12}\cdot 26H_2O$, AFt, and monosulfate, $Ca_4Al_2O_6(SO_4)\cdot 14H_2O$, AFm-14, in hydrothermal hydration of Portland cement and of calcium aluminum oxide–calcium sulfate dihydrate mixtures studied by in situ synchrotron X-ray powder diffraction, J. Solid State Chem. 177 (6) (2004) 1944–1951.
[46] F.P. Glasser, D. Damidot, M. Atkins, Phase development in cement in relation to the secondary ettringite problem, Adv. Cem. Res. 26 (7) (1995) 57–68.
[47] R.B. Perkins, C.D. Palmer, Solubility of ettringite $(Ca_6[Al(OH)_6]_2(SO_4)_3\cdot 26H_2O)$ at 5–75 °C, Geochim. Cosmochim. Acta 63 (13/14) (1999) 1969–1980.
[48] D. Damidot, F.P. Glasser, Thermodynamic investigation of the CaO–Al_2O_3–$CaSO_4$–H_2O system at 50 °C and 85 °C, Cem. Concr. Res. 22 (1992) 1179–1192.
[49] D. Rothstein, J.J. Thomas, B.J. Christensen, H.M. Jennings, Solubility behavior of Ca-, S-, Al-, and Si-bearing solid phases in Portland cement pore solutions as a function of hydration time, Cem. Concr. Res. 32 (10) (2002) 1663–1671.
[50] F.P. Glasser, J. Pedersen, K. Golddthorpe, M. Atkins, Solubility reactions of cement components with NaCl solutions: I Ca(OH)2 and C–S–H, Adv. Cem. Res. 17 (2) (2005) 57–64.
[51] M. Paul, F.P. Glasser, Impact of prolonged warm (85 degrees C) moist cure on Portland cement paste, Cem. Concr. Res. 30 (12) (2000) 1869–1877.
[52] L.J. Parrot, Modelling the development of microstructure, Proc Research on the manufacture and use of cements, Henniker NH, Engineering Foundation, New York, 1986, pp. 43–73.
[53] D.P.H. Hasselman, Relation between effects of porosity on strength and on Young's modulus of elasticity of polycrystalline materials, J. Am. Ceram. Soc. 46 (11) (1963) 564–565.
[54] G.J. Verbeck, R.H. Helmuth, Structure and physical properties of cement paste, Proc 5th Int Symp Chem Cem, Tokyo, 1968, pp. 1–32.
[55] H.M. Jennings, A model for the microstructure of calcium silicate hydrate in cement paste, Cem. Concr. Res. 30 (2000) 101–116.
[56] X. Zhang, Quantitative microstructural characterisation of concrete cured under realistic temperature conditions. Thesis University of Lausanne, 2006.
[57] L.J. Parrot, D.C. Killoh, Prediction of cement hydration, Br. Ceram. Proc. 35 (1984) 41–53.
[58] Y. Gu, C.H. Gammons, M.S. Bloom, A one-term extrapolation method for estimating equilibrium constants of aqueous reactions at elevated temperatures, Geochim. Cosmochim. Acta 58 (17) (1994) 3545–3560.
[59] D.E. Macphee, S.J. Barnett, Solution properties of solids in the ettringite–thaumasite solid solution series, Cem. Concr. Res. 34 (2004) 1591–1598.
[60] C.J. Warren, E.J. Reardon, The solubility of ettringite at 25 °C, Cem. Concr. Res. 24 (8) (1994) 1515–1524.
[61] D. Damidot, F.P. Glasser, Thermodynamic investigation of the CaO–Al_2O_3–$CaSO_4$–H_2O system at 25 °C and the influence of Na_2O, Cem. Concr. Res. 23 (1993) 221–238.
[62] H.A. Berman, E.S. Newman, Heat of formation of calcium aluminate monocarbonate at 25 °C, J. Res. Natl. Bur. Stand., A Phys. Chem. 65A (3) (1961) 197–207.
[63] V. Satava, Determination of standard enthalpies and Gibbs' energies of formation for $6CaO\cdot Al_2O_3\cdot 3SO_3\cdot 32H_2O(C_6A\underline{S}H_{32})$ and 4CaO, $Al_2O_3\cdot 12H_2O(C_4A\underline{S}H_{12})$ by the DHA method, Silikaty 30 (1986) 1–8.
[64] D. Damidot, S. Stronach, A. Kindness, M. Atkins, F.P. Glasser, Thermodynamic investigation of the CaO–Al_2O_3–$CaCO_3$–H_2O closed system at 25 °C and the influence of Na_2O, Cem. Concr. Res. 24 (3) (1994) 563–572.
[65] H. Pöllmann, H. Kuzel, Solid solution of ettringites, Cem. Concr. Res. 20 (1990) 941–947.
[66] P.D. Glynn, MBSSAS: a code for the computation of Margueles parameters and equilibrium relations in binary solid-solution aqueous-solution systems, Comput. Geosci. 17 (7) (1991) 907–966.
[67] P.D. Glynn, E.J. Reardon, L.N. Plummer, E. Busenberg, Reaction paths and equilibrium end-points in solid-solution aqueous-solution systems, Geochim. Cosmochim. Acta 54 (1990) 267–282.
[68] F. Bellmann, On the formation of thaumasite $CaSiO_3\cdot CaSO_4\cdot CaCO_3\cdot 15H_2O$: Part I, Adv. Cem. Res. 16 (2) (2004) 55–60.
[69] M. Schoenitz, A. Navrotsky, Enthalpy of formation of katoite $Ca_3Al_2[(OH)_4]_3$: energetics of the hydrogarnet substitution, Am. Min. 84 (3) (1999) 389–391.
[70] R.B. Peppler, L.S. Wells, The system of lime, alumina, and water from 50° to 250 °C, J. Res. Natl. Bur. Stand. 52 (2) (1954) 75–92.
[71] M.H. Roberts, Synopsis, 5th International Congress on the Chemistry of Cement, vol. 2, 1969, pp. 67–71.
[72] E.T. Carlson, The system lime–alumina–water at 1 °C, J. Res. Natl. Bur. Stand. 61 (1) (1958) 1–11.
[73] F.G. Buttler, H.F.W. Taylor, The system Ca–Al_2O_3–H_2O at 5°, J. Chem. Soc. (1958) 2103–2110.
[74] J. D'Ans, H. Eick, Das System CaO–Al_2O_3–H_2O bei 20 °C und das Erhärten der Tonerdezemente, Zem.-Kalk-Gips 6 (1953) 197–210.
[75] M.T. Faurie-Mounier, Contribution à l'étude du système Ca–Al_2O_3–H_2O, Rev. Mater. Constr. 635–636 (1966) 305–312.
[76] A. Percival, H.F.W. Taylor, Monocalcium aluminate hydrate in the system Ca–Al_2O_3–H_2O at 21°, J. Chem. Soc. (1959) 2629–2631.
[77] L.S. Wells, W.F. Clarke, H.F. McMurdie, Study of the system CaO–Al_2O_3–H_2O at temperature of 21° and 90 °C, J. Res. Natl. Bur. Stand. 30 (1943) 367–409.
[78] H.A. Berman, E.S. Newman, Heat of formation of calcium aluminate monosulfate, J. Res. Natl. Bur. Stand., A Phys. Chem. 67A (1) (1963) 1–13.
[79] F.P. Glasser, A. Kindness, S.A. Stronach, Stability and solubility relationships in AFm phases. Part I. Chloride, sulfate and hydroxide, Cem. Concr. Res. 29 (1999) 861–866.
[80] H. Pöllmann, Solid solution in the system $3CaO\cdot Al_2O_3\cdot SO_4\cdot aq$-$3CaO\cdot Al_2O_3\cdot Ca(OH)4\cdot aq$-$H_2O$ at 25 °C, 45 °C, 60 °C, 80 °C, Neues Jahrb. Mineral. Abh. 161 (1989) 27–40.
[81] R.K. Allada, A. Navrotsky, J. Boerio-Goates, Thermochemistry of hydrotalcite-like phases in the MgO–Al_2O_3–CO_2–H2O system: a determination of enthalpy, entropy, and free energy, Am. Min. 90 (2–3) (2005) 329–335.
[82] A. Emanuelson, S. Hansen, Distribution of iron among ferrite hydrates, Cem. Concr. Res. 27 (8) (1997) 1167–1177.
[83] M. Ecker, Diadochy in calcium aluminoferrates and their hydration products, Hallesches Jahrbuch für Geowissenschaften. B: Geologie Paläontologie, Mineralogie, Halle, Germany, 1998.
[84] G. Möschner, B. Lothenbach, A. Ulrich, R. Figi, R. Kretschmar, Solid solution between Al-ettringite and Fe-ettringite $(Ca_6[Al_{1-x}Fe_x(OH)_6]_2(SO_4)\cdot 26H_2O)$, Cem. Concr. Res. (submitted for publication).
[85] D.A. Kulik, M. Kersten, Aqueous solubility diagrams for cementitious waste stabilization systems: 4. A carbonation model for Zn-doped calcium-silicate hydrate by Gibbs energy minimization, Environ. Sci. Technol. 36 (2002) 2926–2931.
[86] E.P. Flint, L.S. Wells, Study of the system CaO–SiO_2–H_2O at 30 °C and of the reaction of water on the anhydrous calcium silicates, J. Res. Natl. Bur. Stand. 12 (1934) 751–783.
[87] K. Fujii, W. Kondo, Heterogeneous equilibrium of calcium silicate hydrate in water at 30 °C, J. Chem. Soc. Dalton Trans. 2 (1981) 645–651.
[88] P.S. Roller, G. Erwin, The system calcium oxide–silica–water at 30°. The association of silicate ion in dilute alkaline solution, J. Am. Chem. Soc. 62 (3) (1940) 461–471.
[89] S.A. Greenberg, T.N. Chang, Investigation of the colloidal hydrated calcium silicates. II. Solubility relationships in the calcium oxide–silica–water system at 25°, J. Phys. Chem. 69 (1) (1965) 182–188.
[90] A.C. Courault, Simulation experimentale des C–S–H dans les betons modernes: etude de la composition et des proprietes a l'equilibre dans des milieux complexes. Thesis Université de Bourgogne, Dijon, France, 2000.

[91] K.Y. Chen, J.C. Morris, Kinetics of oxidation of aqueous sulfide by O_2, Environ. Sci. Technol. 6 (6) (1972) 529–536.
[92] R. Barbarulo, Compartement des matériaux cimentaires: actions des sulfates et de la temperature. Thesis Université Laval, Quebec, 2002.
[93] H.F.W. Taylor, Hydrated calcium silicates. Part I. Compound formation at ordinary temperatures, Cem. Concr. Res. 726 (1950) 3682–3690.
[94] E. Bonaccorsi, S. Merlino, The crystal structure of tobermorite 14 A (plombierite), a C–S–H phase, J. Am. Ceram. Soc. 88 (3) (2005) 505–512.
[95] M. Atkins, F.P. Glasser, I.P. Moron, J.J. Jack, Thermodynamic modelling of blended cements at elevated temperature (50–90 °C), 1993.
[96] C.L. Dickson, D.R.M. Brew, F.P. Glasser, Solubilities of $CaO–SiO_2–H_2O$ phases at 25°, 55° and 85°C, Adv. Cem. Res. 16 (1) (2004) 35–43.